

## Wind and traffic-induced variation of dynamic characteristics of a cable-stayed bridge – benchmark study

Jae-Hyung Park<sup>a</sup>, Thanh-Canh Huynh<sup>b</sup>, Kwang-Suk Lee<sup>c</sup> and Jeong-Tae Kim<sup>\*</sup>

*Department of Ocean Eng., Pukyong National University, Busan, Korea*

*(Received August 30, 2015, Revised December 11, 2015, Accepted January 5, 2016)*

**Abstract.** A benchmark problem for modal identification of a cable-stayed bridge was proposed by a research team at Hong Kong Polytechnic University. By taking an instrumented cable-stayed bridge as a test bed, nineteen sets of vibration records with known/unknown excitations were provided to invited researchers. In this paper, the vibration responses of the bridge under a series of excitation conditions are examined to estimate the wind and traffic-induced variations of its dynamic characteristics. Firstly, two output-only experimental modal identification methods are selected. Secondly, the bridge and its monitoring system are described and the nineteen sets of vibration records are analyzed in time-domain and frequency-domain. Excitations sources of blind datasets are predicted based on the analysis of excitation conditions of known datasets. Thirdly, modal parameters are extracted by using the two selected output-only modal identification methods. The identified modal parameters are examined with respect to at least two different conditions such as traffic- and typhoon-induced loadings. Finally, the typhoon-induced effects on dynamic characteristics of the bridge are estimated by analyzing the relationship between the wind velocity and the modal parameters.

**Keywords:** cable-stayed bridge; experimental modal analysis; typhoon-induced; traffic-induced; dynamic characteristics

### 1. Introduction

Vibration-based structural health monitoring (SHM) techniques are mostly based on modal parameters such as natural frequencies, damping ratios and mode shapes (Sohn *et al.* 2003, Kim *et al.* 2007a, Koo *et al.* 2009, Kim *et al.* 2011, and Ho *et al.* 2012a). For bridges, forced and ambient vibration tests are commonly utilized to extract modal parameters. With the advantages of low cost, broadband excitation, and no interruption to traffic operation, the ambient vibration test based on natural excitation sources such as wind and traffic has been widely used for SHM of large-scale civil structures (Siringoringo and Fujino 2008, Brownjohn *et al.* 2010, Ho *et al.* 2012b). However, the ambient vibration test does not always provide complete modal parameters, especially mode shapes, due to its dependence on the nature of excitation sources.

Vibration-based SHM techniques aim to evaluate the health status of structures by using the

---

\*Corresponding author, Professor, E-mail: [idis@pknu.ac.kr](mailto:idis@pknu.ac.kr)

<sup>a</sup> BK21Plus Professor

<sup>b</sup> Graduate Student

<sup>c</sup> Graduate Student

change in their modal parameters. It is well known that the modal parameters of structures are affected by structural parameters as well as environmental factors such as temperature and wind (Askegaard and Mossing 1988, Rohrmann *et al.* 2000, Kim *et al.* 2003, Ni *et al.* 2007, Kim *et al.* 2007b, Hong *et al.* 2012, Huynh *et al.* 2015). Many researchers have examined the effect of temperature variation on the modal parameters; meanwhile, only a few studies have been reported on the wind-induced variation of the dynamic features of structures, especially for long-span bridges. Chen *et al.* (2004), Magalhaes *et al.* (2007), Min *et al.* (2009), Kim *et al.* (2014), and Park *et al.* (2015) have reported that natural frequencies of cable-stayed bridges (or suspension bridges) decrease along with the increase in wind speed, and also modal damping ratios exhibit an increasing trend when wind speed increases. In contrast to those reports, Ni *et al.* (2007) reported that natural frequencies of a cable-stayed bridge exhibit increasing trends for most vibration modes as wind speed goes up.

From these previous studies, it seems that the wind-induced variations of dynamic characteristics of cable-stayed bridges are dependent upon the target structures. Ni *et al.* (2015) investigated modal identifiability for Ting Kau Bridge (TKB) under various wind conditions including typhoons by a data-driven stochastic subspace identification (SSI) method; and they concluded that there was a threshold of wind speed that to identify reliable mode shapes. In order to extend the study, the research team led by Prof. Y.Q. Ni at Hong Kong Polytechnic University proposed a benchmark problem for modal identification of the TKB and nineteen sets of vibration records with known/unknown excitation conditions were provided to invited researchers.

In this paper, the vibration responses of the bridge under a series of excitation conditions are examined to estimate the wind and traffic-induced variations of its dynamic characteristics. Firstly, two output-only experimental modal identification methods are selected. Secondly, the bridge and its monitoring system are described and the nineteen sets of vibration records are analyzed in time-domain and frequency-domain. Excitations sources of blind datasets are predicted based on the analysis of excitation conditions of known datasets. Thirdly, modal parameters are extracted by using the two selected output-only modal identification methods. The identified modal parameters are examined with respect to at least two different conditions such as traffic- and typhoon-induced loadings. Finally, the typhoon-induced effects on dynamic characteristics of the bridge are estimated by analyzing the relationship between the wind velocity and the modal parameters.

## 2. Output-only modal analysis methods

To extract modal parameters from output-only vibration responses, modal analysis can be performed in time-domain or frequency-domain. The time-domain methods include Ibrahim time domain (ITD) method (Ibrahim and Mikulcik 1977), eigensystem realization algorithm (ERA) method (Juang and Pappa 1985), stochastic subspace identification and balanced realization (SSI/BR) (Overschee and De Moor 1996), and SSI and canonical variate analysis (SSI/CVA) method (Hermans and Van Der Auweraer 1999). As the frequency-domain methods, peak-peaking (PP) method (Bendat and Piersol, 1993) and frequency domain decomposition (FDD) method (Brinker *et al.* 2000) are broadly used for experimental modal analysis.

From the comparative study by Yi and Yun (2004), two modal identification methods were selected: the first one is the SSI/BR method among the time-domain methods, and the second one is the FDD method among the frequency-domain methods. It is noted that ERA, SSI/BR and

SSI/CVA methods have very similar performances in terms of the accuracy, the computational time and the simplicity. It is also noted that the FDD method has better performance than the PP method.

The stochastic subspace identification (SSI) method utilizes the singular value decomposition (SVD) of a block Hankel matrix with cross correlation matrix of responses. Then a system matrix is obtained by using the result from the SVD, and modal parameters including stable modes, unstable modes and noise modes are calculated by eigenvalue decomposition of the system matrix. Finally, damped frequency ( $\omega_i$ ), damping ratio ( $\xi_i$ ) and mode shape ( $\varphi_i$ ) of the  $i^{th}$  mode are identified by using a stabilization chart as follows (Overschee and De Moor 1996, Yi and Yun 2004)

$$\begin{aligned} \lambda_i &= \frac{1}{\Delta t} \ln \mu_k \\ \omega_i &= -\text{Im}(\lambda_i) / \sqrt{1 - \xi_i^2} \\ \xi_i &= -\text{Re}(\lambda_i) / |\lambda_i| \\ \varphi_i &= \mathbf{C}\Psi_k \end{aligned} \tag{1}$$

where  $\mu_i$  and  $\Psi_i$  are the eigenvalue and the eigenvector from the system matrix, respectively,  $\mathbf{C}$  is an observability matrix from the SVD and  $\Delta t$  is the sampling rate. The frequency domain decomposition (FDD) method utilizes the singular value decomposition of the power spectral density (PSD) matrix  $\mathbf{S}_{yy}(\omega)$  as (Brinker *et al.* 2000, Yi and Yun 2004)

$$\mathbf{S}_{yy}(\omega) = \mathbf{U}(\omega)^T \Sigma(\omega) \mathbf{V}(\omega) \tag{2}$$

where  $\Sigma(\omega)$  is a diagonal matrix containing the singular values  $\sigma_i(\omega)$  ( $i = 1, \dots, n$ ) of its PSD matrix, and  $\mathbf{U}(\omega)$  and  $\mathbf{V}(\omega)$  are unitary matrices.  $\mathbf{U}(\omega)$  is equal to  $\mathbf{V}(\omega)$  since  $\mathbf{S}_{yy}(\omega)$  is symmetric. When peak frequencies in the first singular values  $\sigma_1(\omega)$  are found, mode shapes are extracted from anyone of column vectors of  $\mathbf{U}(\omega_m)$  at the corresponding peak frequencies.

### 3. Vibration records for benchmark study

#### 3.1 Description of Ting Kau Bridge

The TKB is a three-tower cable-stayed bridge with two main spans of 448 m and 475 m respectively, and two side spans of 127 m each. The bridge deck is separated into two carriage-ways with width of 18.8 m each. The bridge deck is supported in the transverse direction at the three towers and in the longitudinal direction only at the central tower. On both ends of the bridge, the deck is vertically connected by rocker bearings into the northern Ting Kau end pier and the southern Tsing Yi abutment. More detailed information of the TKB can be found in Ni *et al.* (2015).

### 3.2 SHM system and measurement records

After the completion of the bridge construction, a long-term monitoring system, called *Wind And Structural Health Monitoring System (WASHMS)*, was instrumented by the Highways Department of the Hong Kong SAR Government to monitor the structural health and performance of the bridge under in-service condition. The details of the WASHMS are described in Karbhari and Ansari (2009).

The layout and geometry design of the accelerometers along the bridge deck on the TKB are shown in Figs. 1 and 2. In Fig. 2, accelerometers (2, 5, 8, 11, 14, 17, 20, and 23) were installed in central cross-girder to measure the transverse acceleration, others were placed on the Ting Kau side deck and the Tsing Yi side deck to measure the vertical acceleration. Also, the anemometers were installed at the deck level of the two main spans and the top of the three towers to measure the wind speed and direction. The anemometer deployment is described in Ni *et al.* (2015). The sampling frequencies set for the accelerometers and the anemometers were 25.6 Hz, and 2.56 Hz, respectively (Ni *et al.* 2015).

As shown in Table 1, total 19 sets monitored from different months and under different wind speeds were provided by the research team at Hong Kong Polytechnic University. As known data, the first 13 datasets (Samples 1-13) of acceleration data were provided with wind speed data. The latter 6 datasets (Samples 14-19) are considered as blind data without provided wind conditions. Samples 1-6 are the data measured under weak wind conditions while Samples 7-10 are the ones measured under strong wind conditions (i.e., typhoons); and Samples 11-13 are measured when the wind speed was about 7.5 m/s. The acceleration responses of the bridge and on-site wind speeds were measured during one hour for all samples. Fig. 3 shows time histories of the vertical acceleration (from Acc.18) and the wind speed for known datasets (Samples 1-13). Note that the wind speed was measured from the WI-GLE-01 station located near Acc. 18 (Ni *et al.* 2015). As shown in the figure, the accelerations for Samples 1 and 3-6 are larger in magnitude than others even though Samples 7-10 are the measured accelerations under typhoons. Fig. 4 shows time histories of vertical acceleration (Acc. 8) for blind datasets (Samples 14-19). It is observed that the acceleration magnitudes for Samples 14-15 are much smaller than others. Among blind datasets, the vibration magnitudes for Sample 18 are the most significant.

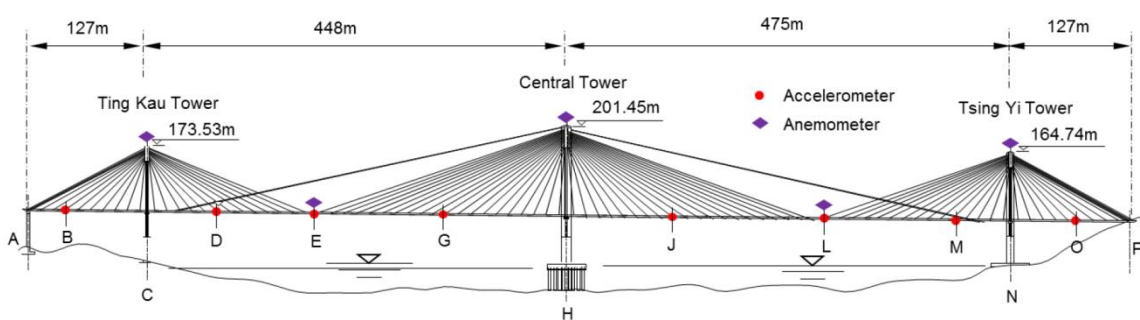


Fig. 1 TKB and layout of accelerometers on bridge deck (Ni *et al.* 2015)

Table 1 Provided 19 data samples under various wind conditions

Wind Condition	Sample	Time duration	Mean hourly wind speed (m/s)	Note
Weak wind	Sample 1	15:00-16:00, 28 Dec 1999	2	
	Sample 2	15:00-16:00, 18 Feb 1999	3.4	
	Sample 3	15:00-16:00, 01 Mar 1999	3.34	
	Sample 4	15:00-16:00, 21 Jun 1999	3.41	
	Sample 5	15:00-16:00, 24 Jul 1999	6.17	
	Sample 6	15:00-16:00, 12 Aug 1999	4.2	
Strong wind (Typhoon)	Sample 7	03:00-04:00, 07 Jun 1999	12.11	Maggie
	Sample 8	02:00-03:00, 23 Aug 1999	15.62	Sam
	Sample 9	06:00-07:00, 16 Sep 1999	21.72	York1
	Sample 10	15:00-16:00, 16 Sep 1999	15.91	York2
≈7.5m/s wind	Sample 11	08:00-09:00, 07 Jun 1999	7.36	
	Sample 12	22:00-23:00, 16 Sep 1999	7.77	
	Sample 13	09:00-10:00, 26 Sep 1999	7.43	
Unknown	Sample 14	1 hour	unknown	
	Sample 15	1 hour	unknown	
	Sample 16	1 hour	unknown	
	Sample 17	1 hour	unknown	
	Sample 18	1 hour	unknown	
	Sample 19	1 hour	unknown	

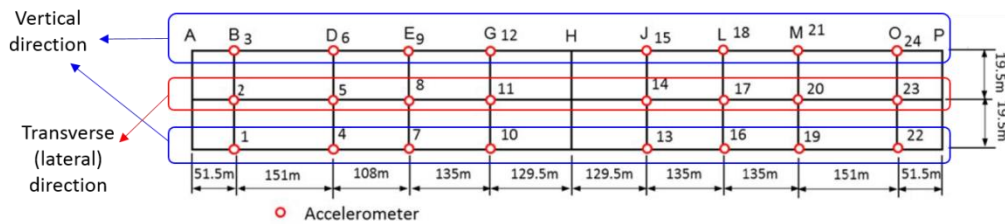
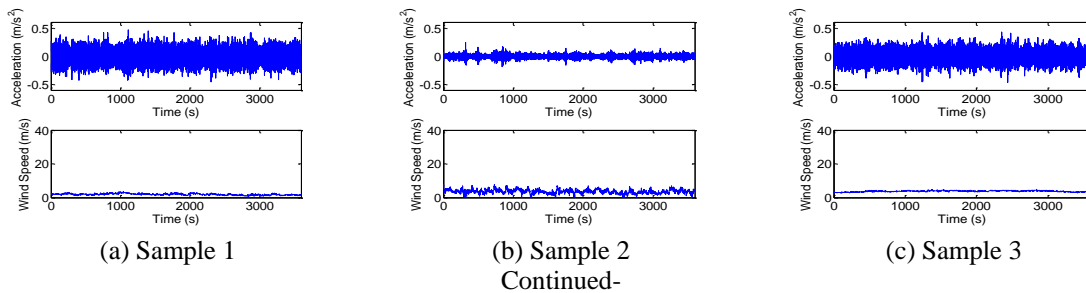


Fig. 2 Geometry configuration of accelerometers on bridge deck (Ni *et al.* 2015)



(a) Sample 1

(b) Sample 2  
Continued-

(c) Sample 3

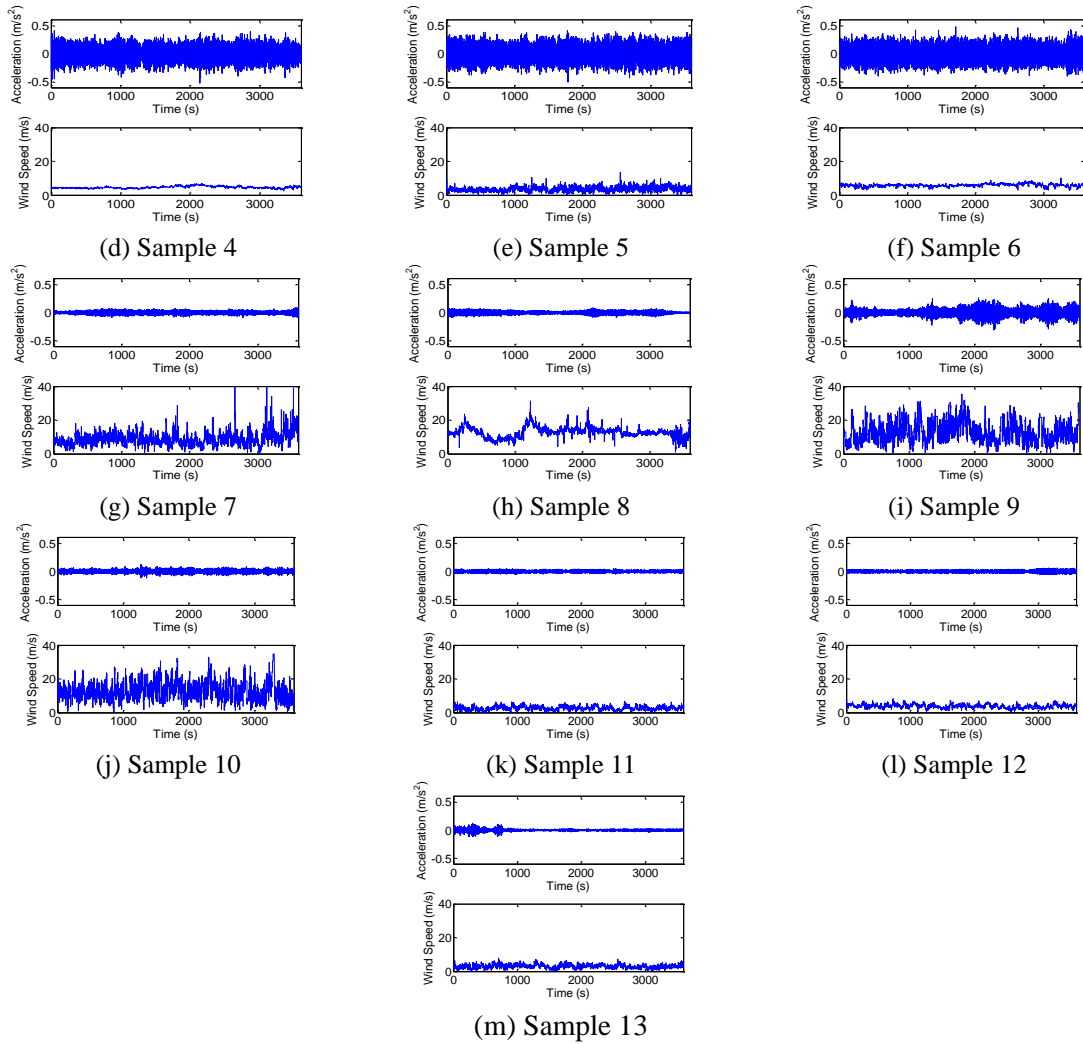


Fig. 3 Time histories of vertical acceleration (Acc. 8) and wind speed (WI-GLE-01) for the known datasets

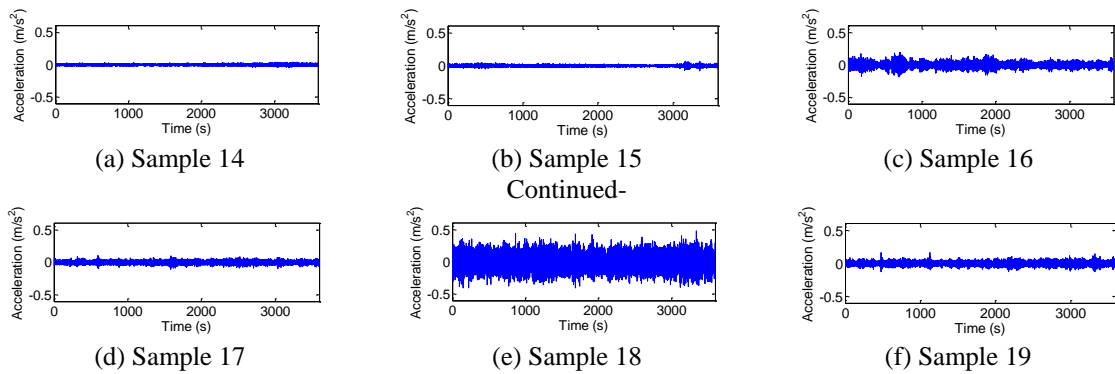


Fig. 4 Time histories of vertical acceleration (Acc. 8) for the blind datasets

### 3.3 Excitation source analysis

As illustrated in Figs. 3 and 4, the excitation forces caused the differences in the magnitudes of the measured acceleration signals. To identify the effect of excitation sources, root-mean-square (RMS) levels of accelerations and mean wind velocities in 100 seconds were analyzed for Samples 1-13 (known datasets). Two acceleration signals measured from Acc.18 installed in the vertical direction (Fig. 5(a)) and Acc.17 installed in the lateral direction (Fig. 5(b)) were examined. Wind speed data measured from the wind station WI-GLE-01 near the accelerometers 17 and 18 were used.

As shown in Fig. 5, the acceleration signals of the 13 Samples were distinguished by two parameters: the RMS level and the mean wind speed. It is observed that Samples 2 and 11-13 belong to the low RMS level and the low wind speed. The low intensity of vibration signals of these Samples might be caused by scarce traffics depending upon the lunar New Year's holidays of year 1999. It is observed that Samples 1 & 3-6 belong to the high RMS levels and the low wind speeds which might be induced by heavy traffics and normal wind conditions. It is also observed that Samples 7-10 belong to the low RMS level of the vertical acceleration signals and the intermediate low-high RMS level of the lateral acceleration signals which might be induced mainly by typhoons.

It is also noticed that the typhoons corresponding to Samples 7-10 caused primarily lateral vibration responses rather than vertical motions, as shown in Fig. 5. The vertical acceleration levels during the typhoons (i.e., Samples 7-10) were relatively lower than the normal traffic days since the traffics might be blocked for the safety of vehicles during the attack of the typhoons. From these observations, the 13 Samples can be categorized into three excitation conditions, as follows:

- 1) *Normal wind and light traffic* condition: Samples 2 & 11-13
- 2) *Normal wind and heavy traffic* condition: Samples 1 & 3-6
- 3) *Strong/typhoon wind* condition: Samples 7-10

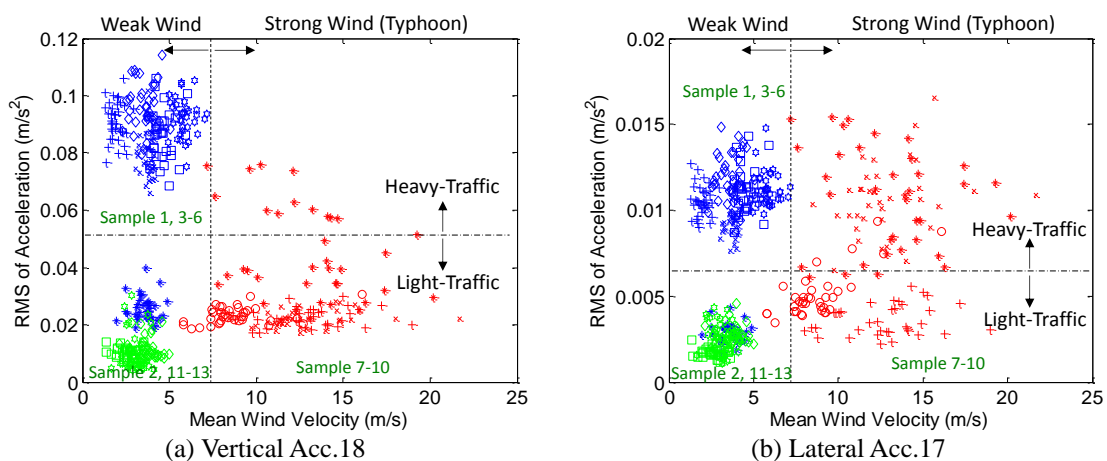


Fig. 5 RMS levels of accelerations under various excitation conditions

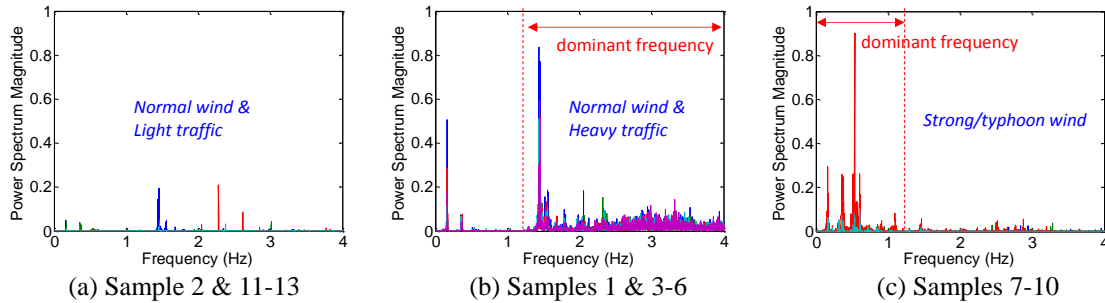


Fig. 6 Power spectrums of the vertical acceleration signals: Acc.18 for the known datasets

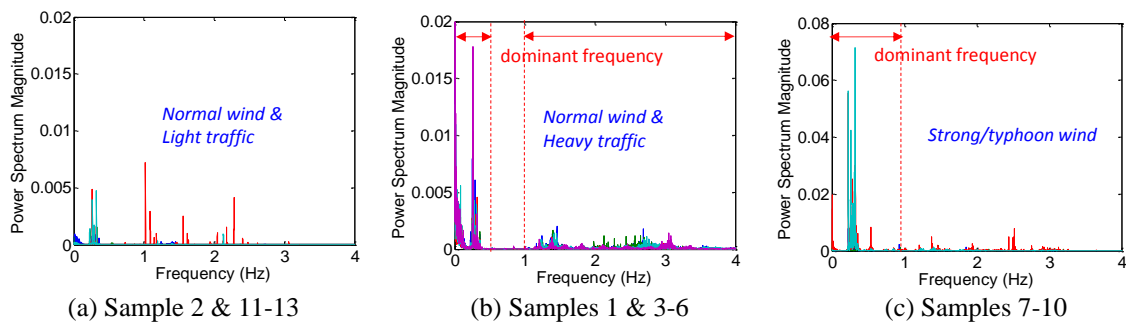


Fig. 7 Power spectrums of the lateral acceleration signals: Acc.17 for the known datasets

Next, power spectrums of the acceleration signals for Samples 1-13 (known datasets) were analyzed to estimate dominant excitation frequencies by the wind and traffic conditions. Fig. 6 shows power spectrums of the vertical acceleration signals (Acc. 18) regarding to the three excitation conditions for the known datasets. As shown in Fig. 6(b), Samples 1 & 3-6 (which can be classified as ‘*normal wind and heavy traffic condition*’) have dominant excitation frequencies above 1 Hz. As shown in Fig. 6(c), Samples 7-10 (which were classified as ‘*strong/typhoon wind condition*’) have dominant excitation frequencies less than 1 Hz.

Furthermore, Fig. 7 shows power spectrums of the lateral acceleration signals (Acc. 17) regarding to the three excitation conditions for the known datasets. It is noted that the lateral frequency responses have similar patterns but small magnitudes compared to those of the vertical frequency responses. However, for Sample 1 & 3-6 (‘*normal wind and heavy traffic condition*’), the dominant frequencies of the lateral acceleration responses were ranged below 0.5 Hz and above 1 Hz.

### 3.4 Excitation source prediction for blind datasets

Power spectrums of the vertical acceleration signals of Acc. 18 for Samples 14-19 (blind datasets) were analyzed to estimate the excitation sources. As shown in Fig. 8, Samples 16-17 have dominant excitation frequencies less than 1 Hz while Samples 18-19 have dominant excitation frequencies above 1 Hz. Relate to the above classification and the observation from Fig. 6, it is predicted that Samples 14-15 were measured under ‘*normal wind and light traffic condition*’ while

Samples 16-17 were measured under ‘*strong/typhoon wind condition*’, and the dominant frequencies of Samples 16-17 were caused by ‘*normal wind and heavy traffic condition*’.

Next, power spectrums of the lateral acceleration signals of Acc. 17 for Samples 14-19 (blind datasets) were also analyzed to estimate the excitation sources. As shown in Fig. 9, Samples 16-17 have dominant excitation frequencies less than 1 Hz while Samples 18-19 have dominant excitation frequencies below 0.5 Hz and above 1 Hz. Relate to the previous classification and the observation from Fig. 7, it is predicted that Samples 14-15 were measured under ‘*normal wind and light traffic condition*’ while Sample 16-17 were measured under ‘*strong/typhoon wind condition*’, and the dominant frequencies of Samples 16-17 were caused by ‘*normal wind and heavy traffic condition*’.

From the observations out of the vertical and lateral vibration signals, the excitation sources of the blind datasets can be classified, as also indicated in Figs. 8 and 9, as follows:

- 1) *Normal wind and light traffic condition*: Samples 14-15
- 2) *Normal wind and heavy traffic condition*: Samples 18-19
- 3) *Strong/typhoon wind condition*: Samples 16-17

#### 4. Experimental modal identification of TKB

##### 4.1 SSI Analysis of dynamic characteristics

As described previously, the SSI method extracts modal parameters by using the stabilization chart. Fig. 10 shows a stabilization chart for Sample 1 when the size of block Hankel matrix was set at  $400 \times 440$ .

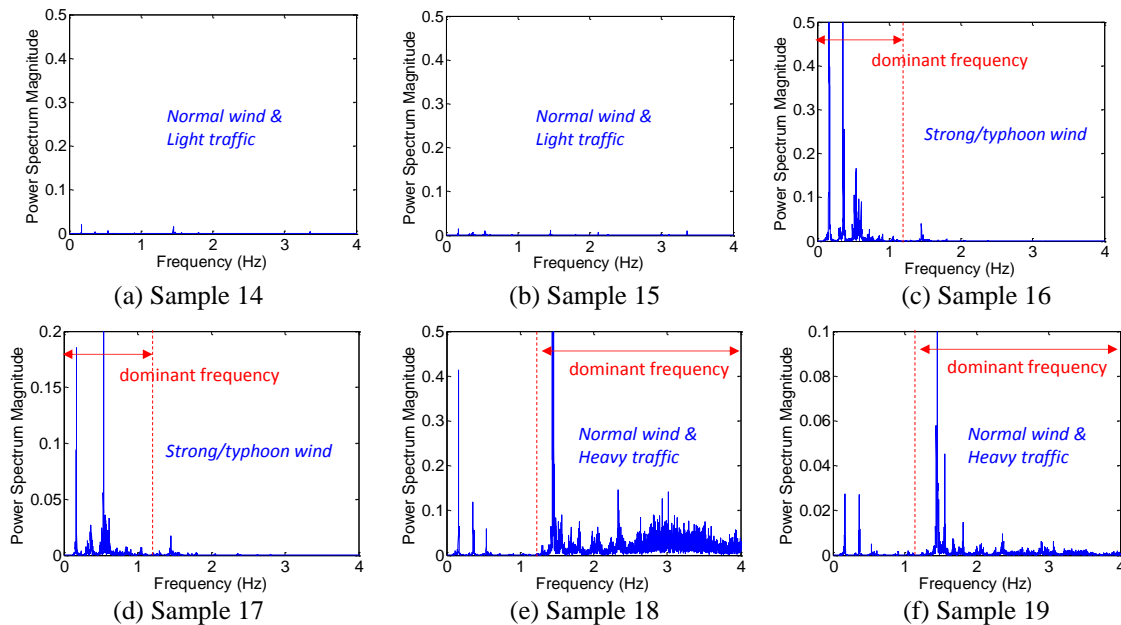


Fig. 8 Excitation source prediction of the blind datasets by power spectrums of the vertical acceleration signals: Acc.18

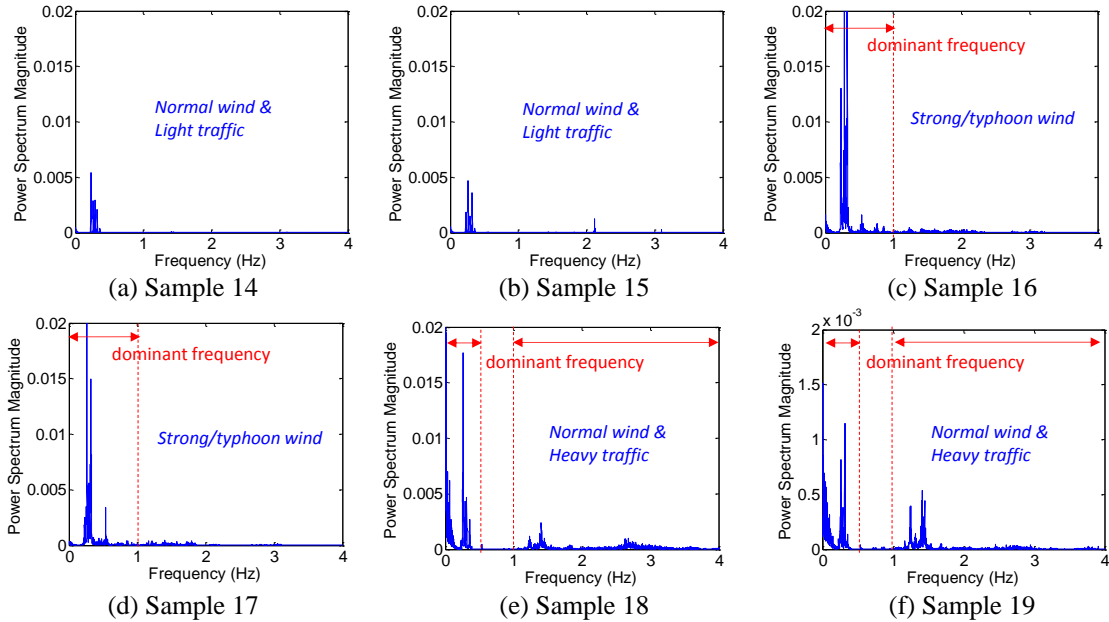


Fig. 9 Excitation source prediction of the blind datasets by power spectrums of the lateral acceleration signals: Acc.17

In the figure, most stable modes are located in the frequency range over than 1 Hz. Only two stable modes can be clearly identified in the frequency range less than 1 Hz. This phenomenon is related to the modal energy of each frequency component. Remind that the vibration energy of Sample 1 is dominant in the frequency range over than 1 Hz, as shown in Fig. 6(b).

In order to identify more stable modes in the frequency range less than 1 Hz, a block Hankel matrix with a huge size is needed. At the same time, the huge memory and storage sizes are also required for the calculation. In this study, a low-pass Butterworth filter was employed to extract stable modes in the frequency range less than 1 Hz. Fig. 11 shows a stabilization chart for Sample 1 after implementing the 4<sup>th</sup> order low-pass filter with a cut-off frequency of 0.7 Hz. As shown in the figure, several stable modes were identified in the frequency range less than 1 Hz.

The cut-off frequency was determined on the basis of numerical analyses of the TKB, which was provided by the research team at The Hong Kong Polytechnic University. Fig. 12(a) show a computed mode shape for the 52<sup>nd</sup> mode (0.6168 Hz) and Fig. 12(b) shows its corresponding normalized mode shapes redrawn for the experimental sensor locations. By comparing two figures (Figs. 12(a) and 12(b)) and considering the existing sensor system on the TKB, the cut-off frequency of the low-pass filter was selected at 0.7 Hz to consider only the modal parameters below the 52<sup>nd</sup> mode. It is noted that the cut-off frequency of the low-pass filter is selected to a higher frequency than the target frequency.

Measured datasets were classified into monitoring directions (i.e., vertical and lateral directions in Fig. 2) in order to conveniently distinguish all modes (i.e., vertical, torsional or lateral mode). For all samples, natural frequencies and damping ratios were extracted by the SSI method.

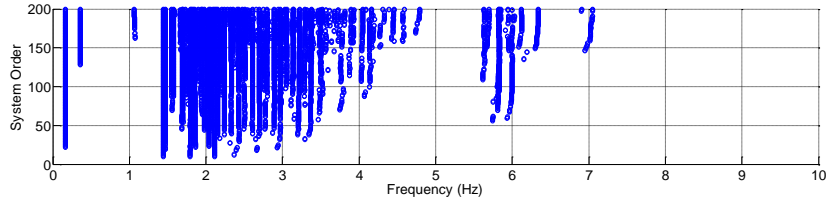


Fig. 10 Stabilization chart for Sample 1 before applying a low-pass filter

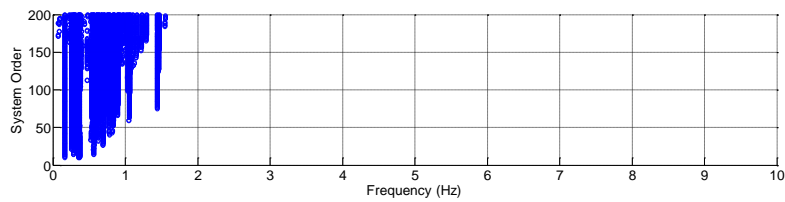


Fig. 11 Stabilization chart for Sample 1 after applying a low-pass filter



(a) Computed mode shape

(b) Computed modal vectors at the sensor locations

Fig. 12 Computed mode shape for 52<sup>nd</sup> mode (0.6168 Hz)

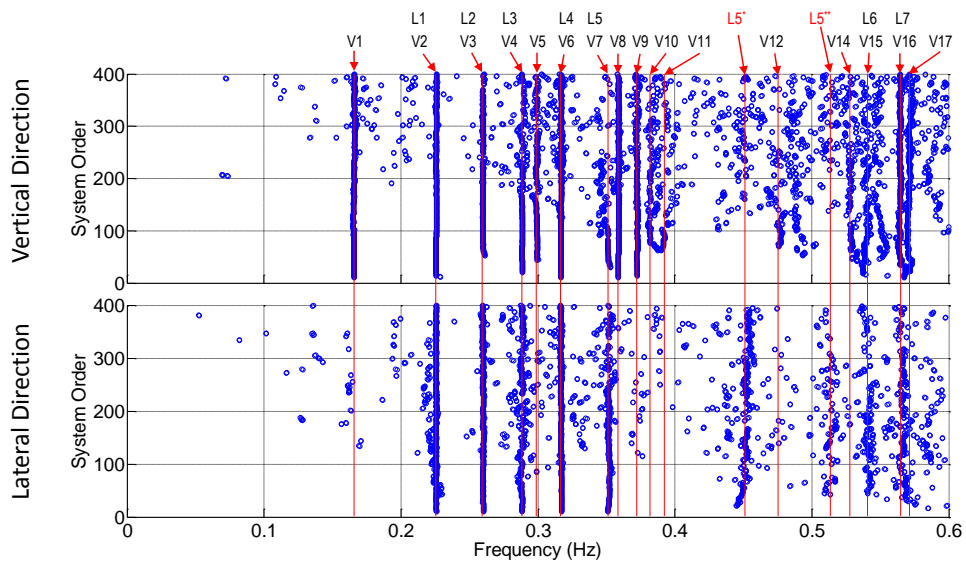


Fig. 13 Separated stabilization charts for Sample 10

Table 2 Extracted natural frequencies (Hz) by SSI in vertical direction

Mode	Sample1	Sample2	Sample3	Sample4	Sample5	Sample6	Sample7	Sample8	Sample9	Sample10
V1	0.1623	0.1623	0.1634	0.1640	0.1638	0.1646	0.1667	0.1640	0.1653	0.1660
V2	-	-	-	-	-	-	0.2269	0.2274	0.2270	0.2259
V3	-	-	-	0.2576	-	0.2595	0.2620	0.2639	-	0.2600
V4	0.2882	0.2902	0.2877	0.2879	0.2852	0.2882	0.2896	0.2915	0.2869	0.2889
V5	0.2998	0.3002	0.2992	0.2992	0.2995	0.2995	0.3006	0.2984	0.3005	0.2994
V6	0.3099	0.3139	0.3113	0.3168	0.3134	0.3197	0.3225	0.3238	0.3199	0.3171
V7	0.3518	0.3578	0.3542	0.3538	0.3511	0.3544	-	0.3688	-	0.3516
V8	0.3586	0.3635	0.3598	0.3592	0.3574	0.3584	0.3613	0.3607	0.3589	0.3592
V9	0.37215	0.3729	0.3720	0.3719	0.3709	0.3724	0.3728	0.3722	0.3730	0.3726
V10	0.3849	0.3819	0.3824	0.3832	-	0.3832	0.3822	-	0.3846	0.3821
V11	0.3969	0.3946	0.3980	0.3947	0.3937	0.3953	0.3924	0.3970	0.3951	0.3920
V12	0.4699	0.4721	0.4702	0.4703	-	0.4659	0.4778	-	-	0.4776
V13	0.4895	-	0.4902	0.4885	-	-	0.4873	0.4835	0.4877	-
V14	0.5335	0.5337	0.5282	0.5328	0.5299	0.5296	0.5272	-	0.5311	0.5287
V15	0.5460	0.5409	0.5375	0.5365	0.5366	0.5366	0.5407	0.5361	0.5369	0.5397
V16	0.5633	0.5655	0.5658	0.5634	0.5628	0.5640	0.5655	0.5651	0.5650	0.5647
V17	0.5699	0.5703	0.5712	0.5698	0.5683	0.5700	0.5725	0.5719	0.5735	0.5717
Mode	Sample11	Sample12	Sample13	Sample14	Sample15	Sample16	Sample17	Sample18	Sample19	
V1	0.1681	0.1652	0.1689	0.1688	0.1686	0.1644	0.1667	0.1631	0.1629	
V2	0.2295	0.2277	0.2273	0.2274	0.2281	0.2272	0.2275	-	-	
V3	-	0.2638	0.2636	0.2646	0.2639	-	0.2617	0.2561	-	
V4	0.2824	0.2895	0.2910	0.2908	0.2906	0.2824	0.2887	0.2889	0.2873	
V5	0.2999	0.2997	0.3011	0.3011	0.3011	0.3009	0.2996	0.2998	0.2994	
V6	0.3281	0.3223	0.3230	0.3226	0.3214	0.3213	0.3206	0.3110	0.3146	
V7	-	0.3553	0.3682	0.3647	0.3656	-	-	0.3520	0.3544	
V8	0.3603	0.3619	0.3604	0.3605	0.3599	0.3576	0.3590	0.3596	0.3602	
V9	0.3734	0.3737	0.3746	0.3753	0.3736	0.3715	0.3721	0.3733	0.3729	
V10	0.3790	-	0.3840	0.3900	0.3819	-	0.3815	0.3862	0.3845	
V11	0.3970	0.3930	0.3970	0.3966	0.3904	0.3920	0.3979	0.3952	0.3951	
V12	0.4660	-	-	0.4887	0.4868	0.4637	0.4794	0.4662	0.4735	
V13	-	0.4852	0.4825	-	-	-	-	0.4925	0.4822	
V14	0.5305	0.5298	0.5316	0.5309	0.5295	0.5274	0.5296	0.5300	0.5306	
V15	0.5370	0.5393	0.5389	0.5404	0.5398	0.5377	0.5383	0.5374	0.5377	
V16	0.5668	0.5657	0.5670	0.5664	0.5665	-	0.5648	0.5639	0.5642	
V17	0.5720	0.5730	0.5739	0.5734	0.5740	0.5723	0.5730	0.5699	0.5702	

Table 3 Extracted damping ratios (%) by SSI in vertical direction

Mode	Sample1	Sample2	Sample3	Sample4	Sample5	Sample6	Sample7	Sample8	Sample9	Sample10
V1	0.9147	1.0817	1.2838	0.8708	1.3748	1.9161	1.5714	1.6965	2.6236	1.6952
V2	-	-	-	-	-	-	0.6500	0.7036	0.4500	0.6561
V3	-	-	-	2.2562	-	1.9161	0.9562	0.8720	-	1.1947
V4	1.1050	0.9063	1.3116	1.1457	1.8803	3.4157	1.1310	1.6718	1.4480	1.9898
V5	0.9287	0.6042	0.8404	0.9486	0.9339	1.3184	1.1475	1.2875	1.2185	1.6100
V6	0.7261	0.6970	1.1102	0.9479	1.2795	1.0603	0.8713	0.8478	1.5316	0.9897
V7	1.3287	0.6965	1.8191	1.3021	1.6553	3.1956	-	1.5698	-	2.3124
V8	0.7972	0.9370	0.9279	1.0888	0.7438	0.8252	1.1812	1.0642	0.9771	0.7714
V9	0.5624	0.5419	0.4287	0.5329	0.7412	0.5755	1.0288	0.7220	0.9305	0.7234
V10	1.5544	0.6162	0.7213	0.7039	-	1.4781	0.7589	-	1.2386	1.3573
V11	1.4091	1.9837	0.9225	1.1020	0.7375	1.0811	1.7177	1.4071	1.2586	1.3754
V12	2.8790	2.0424	3.0483	2.6170	-	2.6923	2.7812	-	-	2.9642
V13	1.0871	-	1.1967	1.0908	-	-	1.2924	1.3651	1.8005	-
V14	1.9421	1.0022	0.6817	0.9736	0.6268	0.6193	0.6465	-	0.6433	0.8026
V15	0.7612	1.5967	1.2483	1.2624	1.1797	1.4922	1.3923	1.1892	1.0271	1.4237
V16	0.7378	0.7230	0.6084	0.7133	0.6354	0.4806	0.6879	0.4060	0.5193	0.5114
V17	0.7545	0.5281	0.7636	1.1216	0.9797	1.1817	1.1243	0.8517	1.2954	0.9744
Mode	Sample11	Sample12	Sample13	Sample14	Sample15	Sample16	Sample17	Sample18	Sample19	
V1	1.4363	1.1463	0.9991	1.0605	1.2284	2.2665	1.7022	1.1337	1.9047	
V2	0.8596	1.0252	0.6246	0.3483	0.4874	1.4121	1.6466	-	-	
V3	-	0.6320	1.1847	0.6558	0.7716	-	0.8505	2.9677	-	
V4	1.1083	0.9424	0.5482	0.4380	0.6872	1.3262	2.4950	0.8987	1.6043	
V5	1.0776	0.9981	0.9895	0.5710	0.9413	1.0594	2.0268	1.0731	1.1573	
V6	1.1621	0.8144	0.4361	0.5451	0.5929	1.8638	1.2944	1.0138	0.7909	
V7	-	2.6291	1.5068	1.0825	1.2368	-	-	1.6000	4.0840	
V8	0.5936	0.6436	0.9618	0.7204	0.6744	0.8348	1.1636	0.6677	0.9079	
V9	0.5421	0.6548	1.2119	0.5931	0.4362	0.6715	0.9355	0.6034	0.6047	
V10	0.9113	-	1.4582	0.7451	0.9553	-	0.9987	1.0312	1.6879	
V11	2.4177	1.6258	0.7469	1.5021	0.8294	1.6716	1.6963	0.9077	1.9911	
V12	1.8461	-	-	2.0569	1.9953	2.5998	3.2042	2.6407	2.2443	
V13	-	1.6939	0.8559	-	-	-	-	1.8980	1.4043	
V14	1.0316	0.4365	0.3892	0.7820	0.6391	0.6008	0.5351	0.6119	0.8791	
V15	1.5719	1.3606	1.9776	1.1701	1.1779	1.2641	0.8268	0.9249	1.3007	
V16	0.8668	0.4509	0.4826	0.3099	0.3484	-	0.4569	0.4872	0.9420	
V17	0.8225	0.9325	0.9959	0.8194	0.7635	1.0289	1.1539	0.8730	0.5552	

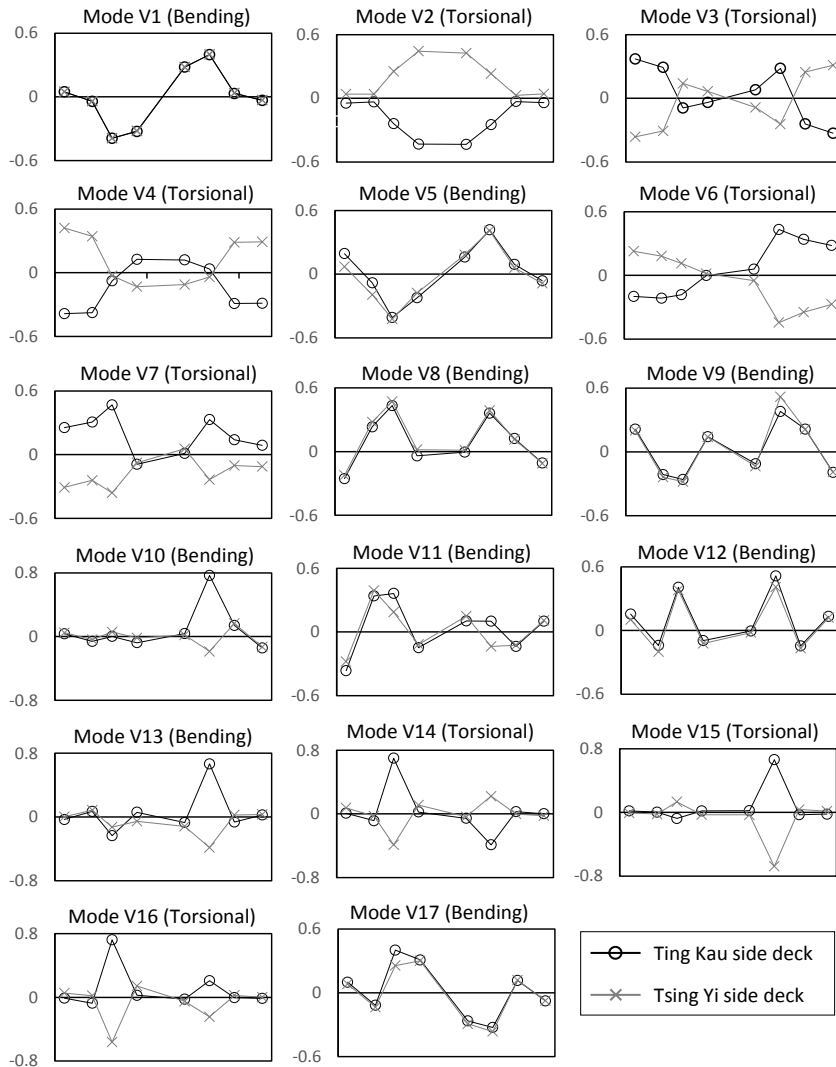


Fig. 14 Extracted mode shapes in vertical direction by SSI

From the acceleration data measured in the vertical direction, seventeen (17) vertical modes (Modes V1-V17) were identified from the stabilization chart for Sample 10, as shown in Fig. 13. The identified natural frequencies and damping ratios of these seventeen modes are listed in Tables 2 and 3, and the corresponding mode shapes are shown in Fig. 14. In the figure, the mode shape pairs with opposite sign are torsional modes, and the others are vertical bending modes. As observed from Fig. 14, V1, V5, V8, V9, V10-V13 and V17 are vertical bending modes and the others are torsional modes. It is noticed in the tables that Modes V2 and V3 cannot be extracted from Samples 1-6 & 18-19 (traffic dominant conditions), but were identified from other samples (wind dominant conditions).

Table 4 Extracted natural frequencies (Hz) by SSI in lateral direction

Mode	Sample1	Sample2	Sample3	Sample4	Sample5	Sample6	Sample7	Sample8	Sample9	Sample10
L1	0.2266	0.2279	0.2269	0.2286	0.2253	0.2221	0.2265	0.2268	0.2270	0.2258
L2	0.2574	0.2593	0.2598	0.2584	0.2579	0.2605	0.2627	0.2639	0.2594	0.2601
L3	0.2883	0.2901	0.2882	0.2879	0.2859	0.2872	0.2898	0.2904	0.2860	0.2884
L3*	-	-	-	-	-	-	-	0.3004	-	-
L3**	-	-	-	-	-	-	-	-	0.3114	-
L4	0.3097	0.3145	0.3110	0.3165	0.3154	0.3200	0.3224	0.3238	0.3213	0.3170
L4*	-	-	-	-	-	-	-	-	0.3353	-
L5	0.3548	0.3584	0.3562	0.3560	0.3548	0.3546	0.3606	0.3701	0.3605	0.3519
L5*	-	-	-	-	-	-	-	-	-	0.4522
L5**	-	-	-	-	-	-	-	-	-	0.5134
L6	-	0.5442	0.5393	0.5367	0.5347	0.5376	0.5390	0.5385	0.5373	0.5413
L7	0.5661	0.5668	0.5666	0.5640	0.5626	0.5656	0.5657	0.5663	0.5659	0.5671

Mode	Sample11	Sample12	Sample13	Sample14	Sample15	Sample16	Sample17	Sample18	Sample19
L1	-	0.2270	0.2273	0.2275	0.2282	-	0.2269	0.2272	0.2278
L2	0.2297	0.2638	0.2644	0.2646	0.2638	0.2303	0.2615	0.2587	0.2587
L3	0.2826	0.2889	0.2911	0.2908	0.2908	0.2820	-	0.2888	0.2905
L3*	-	-	-	-	-	-	0.2901	-	-
L3**	-	-	-	-	-	-	-	-	-
L4	0.3145	0.3220	0.3231	0.3226	0.3225	0.3138	0.3214	0.3108	0.3151
L4*	0.3285	-	-	-	-	0.3221	-	-	-
L5	0.3603	0.3608	0.3671	0.3636	0.3632	0.3579	0.3589	0.3560	0.3575
L5*	-	-	-	-	-	-	-	-	-
L5**	-	-	-	-	-	0.5252	-	-	-
L6	0.5443	0.5390	-	0.5395	0.5412	0.5381	0.5382	0.5362	0.5399
L7	0.5685	0.5644	0.5675	0.5670	0.5679	-	0.5649	0.5662	0.5655

For the measured acceleration data in the lateral direction, the natural frequencies and damping ratios of seven (7) lateral modes (Modes L1-L7) were identified from the stabilization chart for Sample 10 (see Fig. 13) and listed in Tables 4 and 5. In the tables, asterisk symbols indicate additional lateral modes appeared in special conditions (e.g., typhoons). The lateral motions corresponding to the modes L1-L7 and the additional modes L3\*, L3\*\*, L4\*, L5\* and L5\*\* were extracted as shown in Fig. 15. The additional lateral modes were appeared in Samples 8-10 & 16-17 (*strong/typhoon wind* condition): (1) Mode L3\* for Sample 8 (Typhoon Sam), (2) Modes

L3\*\* and L4\* for Sample 9 (Typhoon York1), (3) Modes L5\* and L5\*\* for Sample 10 (Typhoon York 2), (4) Mode L4\* and Mode L5\*\* for Sample 16, and (5) Mode L3\* for Sample 17. From these observations, it is found that the additional five lateral modes are appeared only in the *strong/typhoon wind* condition and their occurrences may depend on frequency characteristics of the wind. It is noted that the excitation sources for Samples 16 and 17 were predicted as the *strong/typhoon wind* condition in the previous section.

Table 5 Extracted damping ratios (%) by SSI in lateral direction

Mode	Sample1	Sample2	Sample3	Sample4	Sample5	Sample6	Sample7	Sample8	Sample9	Sample10
L1	0.5758	1.8692	0.9435	1.1198	1.3589	1.4830	0.5113	0.5049	0.5571	0.8776
L2	1.3973	1.3508	0.9847	0.8174	2.7692	0.6562	0.8205	0.8109	2.4492	1.1897
L3	0.9988	0.7288	1.1242	0.8201	1.6968	1.6968	1.1670	1.2219	1.3662	1.8417
L3*	-	-	-	-	-	-	-	1.7249	-	-
L3**	-	-	-	-	-	-	-	-	1.5659	-
L4	0.6316	0.6386	1.0090	0.8703	1.0948	0.9194	0.9240	0.8028	1.2635	1.0317
L4*	-	-	-	-	-	-	-	-	2.1595	-
L5	1.2025	1.0398	1.3888	1.6587	2.1402	2.5228	2.6624	1.3162	1.6442	2.7097
L5*	-	-	-	-	-	-	-	-	-	2.0874
L5**	-	-	-	-	-	-	-	-	-	1.9642
L6	-	1.7959	1.3701	1.4109	1.1474	1.2058	1.0533	1.8317	1.1890	1.6870
L7	0.9223	0.5969	0.9980	0.7311	0.7161	0.6941	0.4008	0.5473	0.6690	1.1145
Mode	Sample11	Sample12	Sample13	Sample14	Sample15	Sample16	Sample17	Sample18	Sample19	
L1	-	1.1219	0.6567	0.3787	0.5005	-	2.2877	0.6031	1.0093	
L2	0.7331	0.6586	0.5830	0.5873	0.7151	2.4097	0.8441	0.9387	2.1361	
L3	1.2924	1.3346	0.5180	0.4781	0.6881	1.2651	-	0.8025	1.2310	
L3*	-	-	-	-	-	-	2.5533	-	-	
L3**	-	-	-	-	-	-	-	-	-	
L4	1.0705	0.9902	0.4810	0.6234	0.6970	1.3975	1.3723	0.7669	0.7193	
L4*	1.0560	-	-	-	-	1.8246	-	-	-	
L5	0.9689	1.7337	1.6380	1.0120	1.1591	2.6841	2.5180	1.0499	2.9475	
L5*	-	-	-	-	-	-	-	-	-	
L5**	-	-	-	-	-	1.1200	-	-	-	
L6	1.8068	1.3655	-	1.4768	1.6512	1.5655	1.3218	1.0773	1.2851	
L7	0.9676	0.5638	0.5836	0.5209	0.6059	-	0.4838	0.5953	1.1741	

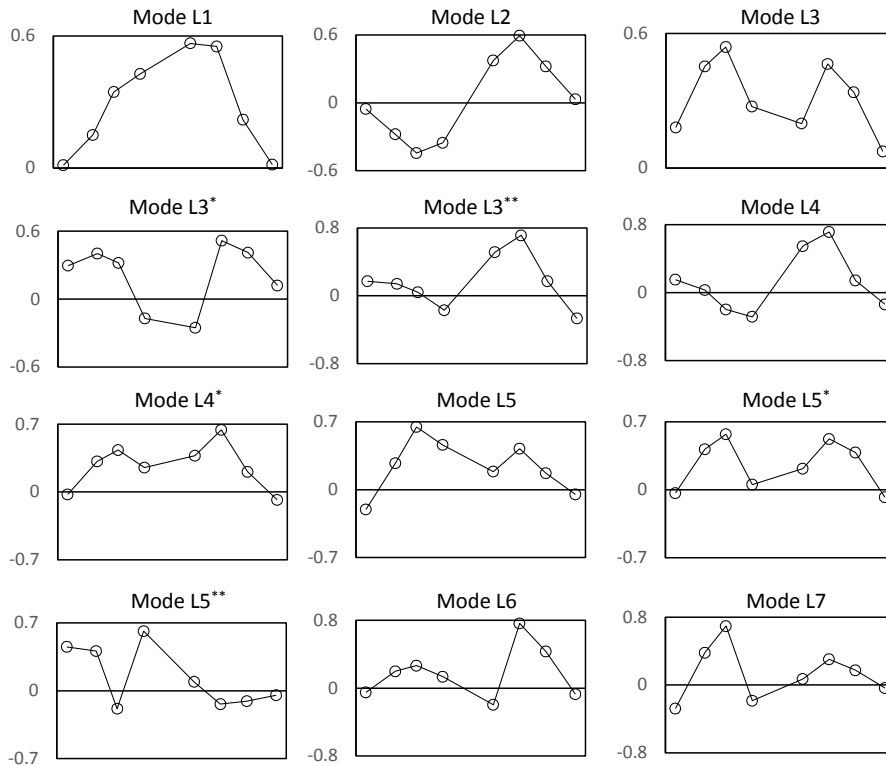


Fig. 15 Extracted mode shapes in lateral direction by SSI

In order to compare with the results by Ni *et al.* (2015), experimental modal analyses were performed for all samples by analyzing the vertical and lateral acceleration data at the same time. Note that the similar manner was used by Ni *et al.* (2015). Fig. 16 shows a stabilization chart for Sample 10, and the identified modes were compared with the results by Ni *et al.* (2015) as listed in Table 6. From the stabilization chart shown in Fig. 16, an extra mode was clearly identified between Mode 6 and Mode 7. It is noted that the mode order in Fig. 16 follows the reference Ni *et al.* (2015). In this study, the extra mode is identified as Mode V7L5 (coupled torsional and lateral mode) located between Mode V6L4 (coupled torsional and lateral mode) and Mode V8 (vertical mode), see Table 6.

The vertical modal vectors of the extra mode (Mode V7L5) were extracted for all samples, as shown in Fig. 17. It is observed that some identified vertical mode shapes (see Fig. 17) are similar to the torsional motion V7 (see Fig. 14), and the others are similar to the vertical bending motion V8 (see Fig. 14). In addition, the separated stabilization charts of the vertical and lateral accelerations for Sample 10 (see Fig. 13) indicates that the extra mode (Mode V7L5) is obviously matched to the torsional motion V7 (see Fig. 14) and the lateral motion L5 (see Fig. 15). Therefore, the vertical mode shapes of Mode V7L5 and Mode V8 could be overlapped under different excitation conditions. Furthermore, Ni *et al.* (2015) might consider the extra mode (V7L5) as a noise mode because its mode shape in the vertical direction does not have a consistency for all samples, see Fig. 17.

For further observations on the inconsistency of the extra mode, the natural frequencies for Mode V7L5 and V8 identified in this study were investigated by tracking their changes for various wind conditions as plotted in Fig. 18. It is observed that Mode V7L5 shifted over Mode V8 for Samples 8, and 13~15. Among all identified modes of the TKB, the shift of the modal order was observed only for Mode V7L5 and Mode V8. For all samples, the absolute differences in the natural frequency between the lateral mode L5 and the vertical mode V8 are plotted in Fig. 19. It is observed that the natural frequencies of the vertical mode V7 and the lateral mode L5 are quite close to those of the vertical mode V8 for Samples 1-6, 7, 9, 11-12, and 14-19, but they are different for Samples 8, 10 and 13. It is also observed that the mode shape of the vertical mode V7 depends on the difference in the natural frequencies between the modes L5 and V8.

Table 6 Mode's classifications (this study vs Ni *et al.* 2015)

Ni <i>et al.</i> (2015)		This study		
Mode No.	Description	Mode No.		Description
		Vertical	Lateral	
1	Predominantly vertical mode	V1	-	Vertical mode
2	Coupled torsional & lateral mode	V2	L1	Coupled torsional & lateral mode
3	Predominantly lateral mode	V3	L2	Coupled torsional & lateral mode
4	Coupled torsional & lateral mode	V4	L3	Coupled torsional & lateral mode
5	Predominantly vertical mode	V5	-	Vertical mode
6	Coupled torsional & lateral mode	V6	L4	Coupled torsional & lateral mode
-	-	V7	L5	Coupled torsional & lateral mode
7	Predominantly vertical mode	V8	-	Vertical mode
8	Predominantly vertical mode	V9	-	Vertical mode
9	Predominantly vertical mode	V10	-	Coupled vertical & torsional mode
10	Predominantly vertical mode	V11	-	Vertical mode
		V12	-	Vertical mode
		V13	-	Coupled vertical & torsional mode
		V14	-	Torsional mode
		V15	L6	Coupled torsional & lateral mode
		V16	L7	Coupled torsional & lateral mode
		V17	-	Vertical mode

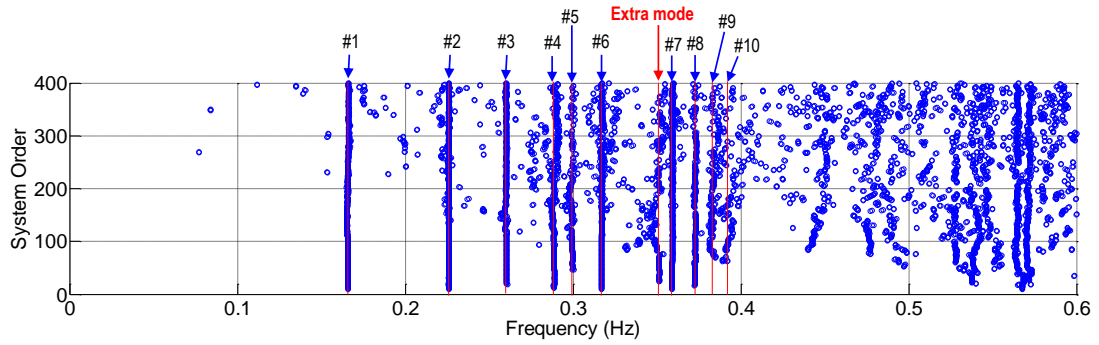


Fig. 16 Stabilization chart plotted by using both the vertical and lateral acceleration data for Sample 10

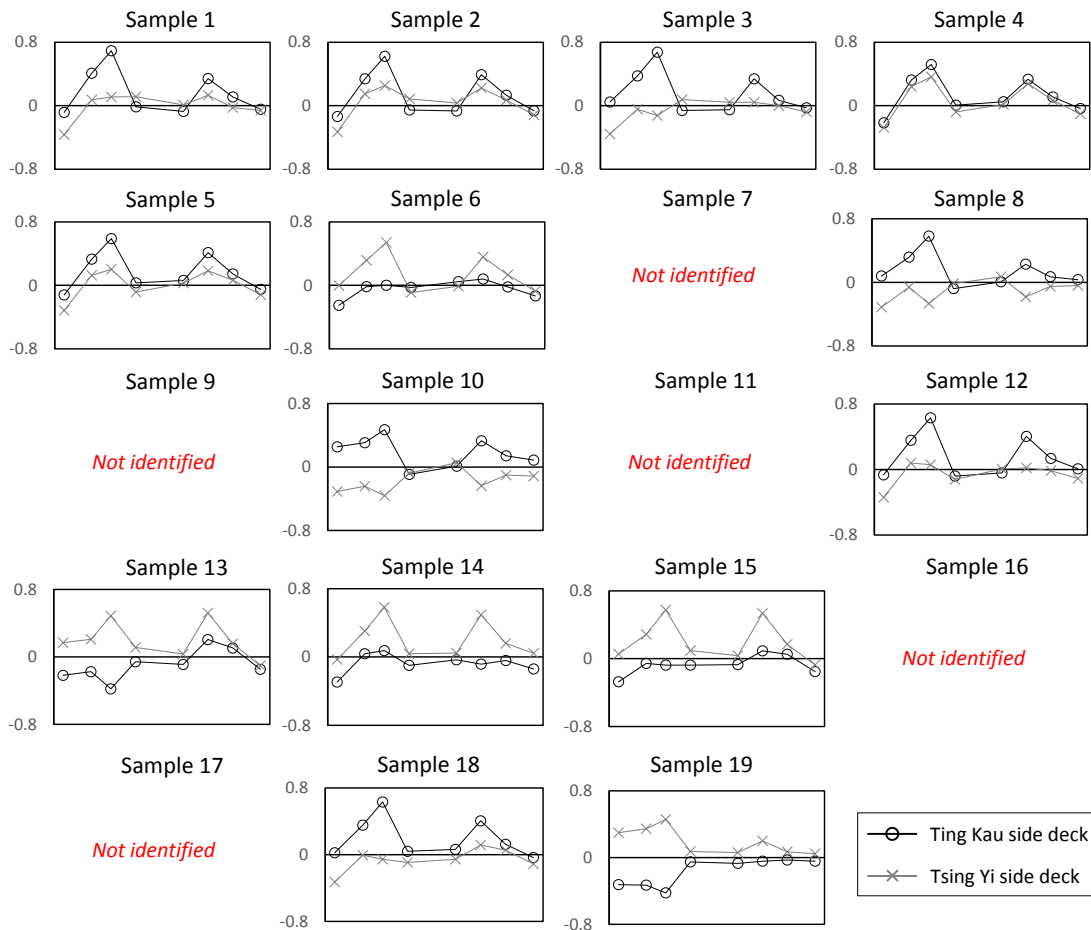


Fig. 17 Vertical modal vectors of extra mode (V7L5) extracted by using vertical and lateral accelerations at the same time

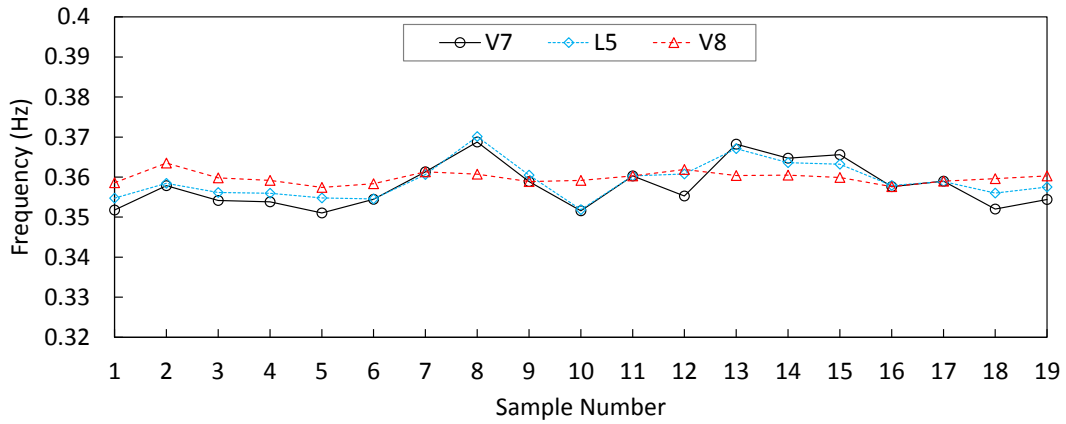


Fig. 18 Frequency variations among vertical mode V7, lateral mode L5, and vertical mode V8

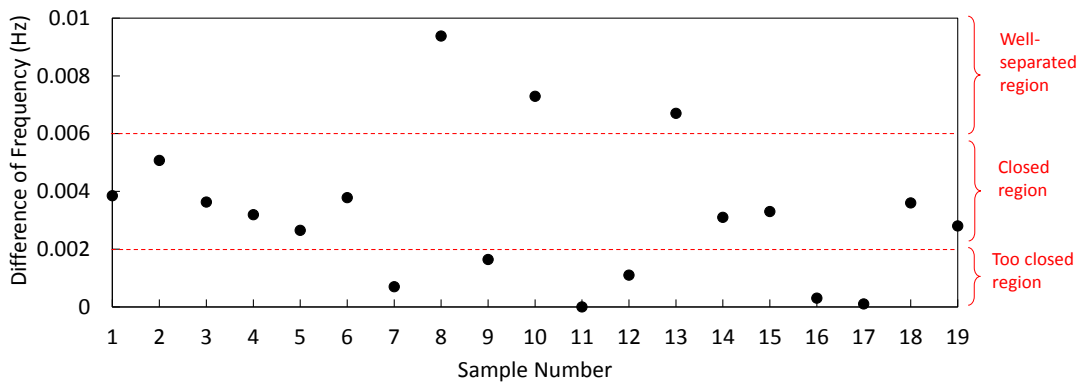


Fig. 19 Absolute differences in natural frequencies between lateral mode L5 and vertical mode V8

#### 4.2 FDD Analysis of dynamic characteristics

To compare the performance of the modal identifiability, the modal parameters were also extracted by the FDD method. FFT length to construct the PSD matrix was set to  $2^{15}$  (=32,768) and an overlapping of 66 % was used. With these setup, the frequency resolution was 0.00078125 Hz. The modal parameters were also separately extracted for the vertical and lateral directions. Figure 20 shows the singular value chart in each direction for Sample 10. As observed from the figure, there exists several clear peaks and a number of less clear ones in each singular value chart. Among them, only peaks corresponding to the modes identified by the SSI method were selected to compare the performance. It is noted that the FDD method selected in this study cannot extract damping ratio.

For all samples, the natural frequencies and the mode shapes were extracted for each separated direction. From the acceleration data measured in the vertical direction, the natural frequencies of

seventeen (17) vertical modes (Modes V1-V17) were identified as listed in Tables 7. From the vibration records in the lateral direction, the natural frequencies of seven (7) lateral modes (Modes L1-L7) were identified as listed in Tables 8. In the tables, asterisk symbols indicate the additional lateral modes which were identified by the SSI method. Compared with the results by the SSI method, the FDD method identified less modes for all samples. Especially, the FDD method failed to identify the torsional mode V7L5.

In order to compare the accuracy of the extracted mode shapes for the two modal identification methods, the consistency of the mode shapes was examined for each method. For the examination, the modal assurance criterion (MAC) value are employed as

$$MAC_{i,j} = \frac{[\phi_i^T \phi_j]}{[\phi_i^T \phi_i][\phi_j^T \phi_j]} \tag{3}$$

where  $\phi_i$  and  $\phi_j$  are the mode shapes for Sample  $i$  and  $j$ .

MAC values of two coupled modes (Modes V2L1 and V3L2) and two vertical modes (Modes V5 and V9) were examined for all samples, as shown in Fig. 21. For each MAC value, the mode shape for Sample 7 was used as the reference. Note that MAC values were set as 0 for unidentified modes. It is observed that the mode shapes extracted by the SSI method have the higher consistency than the FDD method for all samples. It is also observed that the vertical mode shapes (Modes V5 and V9) extracted by the FDD method have very low accuracy for Samples 8-10, and 16-17 (corresponding to typhoon-induced wind conditions). It is concluded that the SSI method is more reliable than the FDD method when modal parameters of large structures are extracted by ambient tests such as Sample 7-10 & 16-17 of this study.

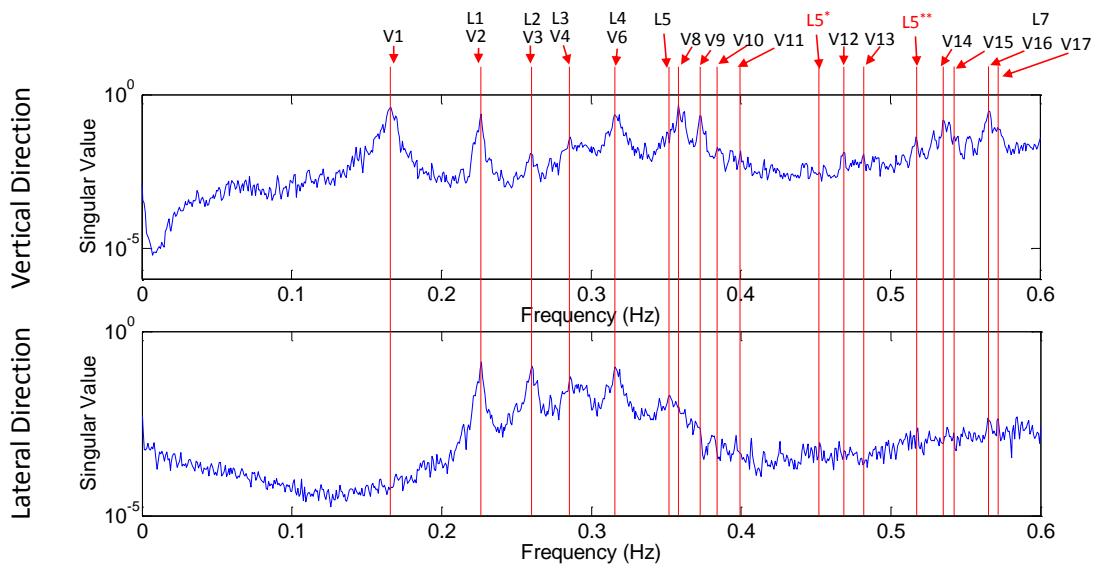


Fig. 20 Singular value charts and identified modes by FDD for Sample 10

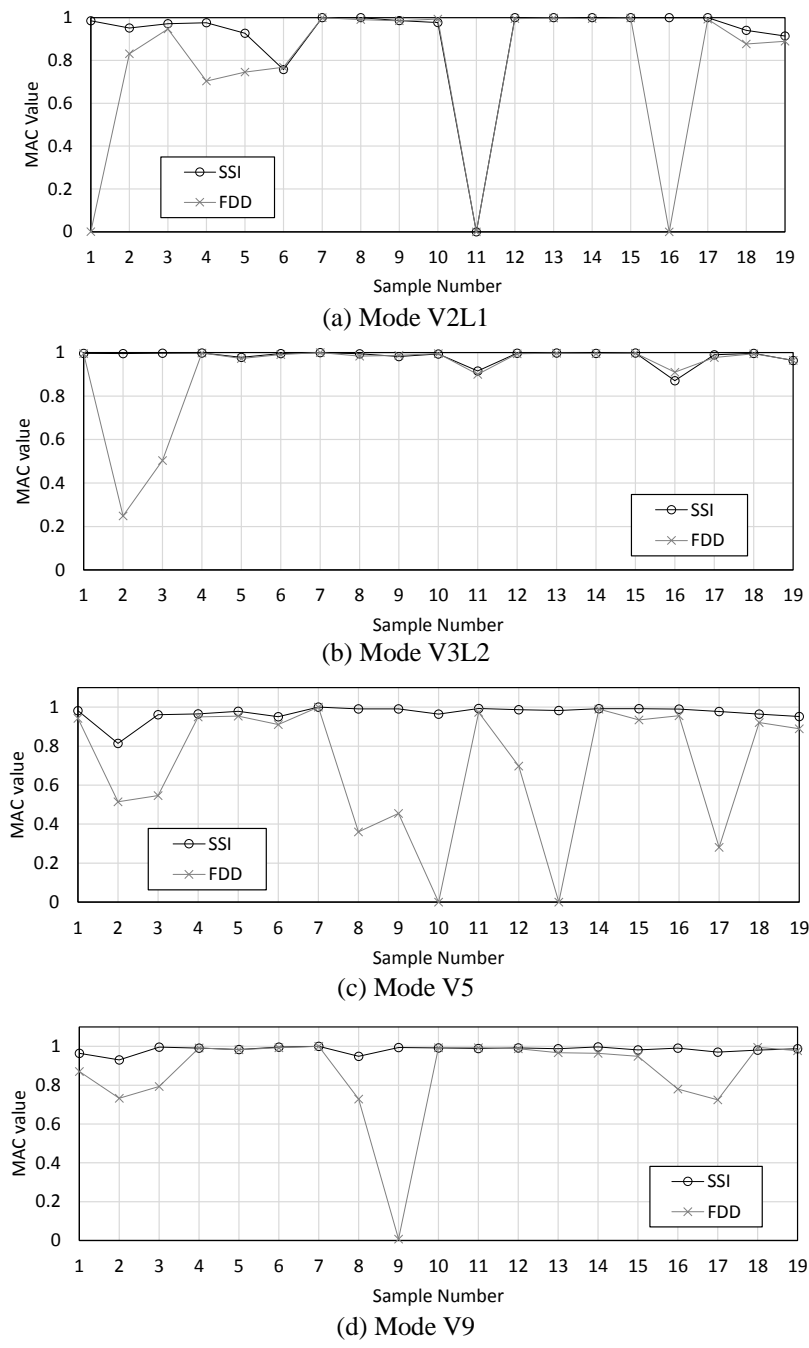


Fig. 21 MAC value variations of mode shapes extracted by SSI and FDD

Table 7 Extracted natural frequencies (Hz) by FDD in vertical direction

Mode	Sample1	Sample2	Sample3	Sample4	Sample5	Sample6	Sample7	Sample8	Sample9	Sample10
V1	0.1625	0.1625	0.1625	0.16406	0.16406	0.16563	0.16641	0.16172	0.1625	0.16641
V2	0.22734	-	0.22813	-	-	-	0.22656	0.22734	0.22656	0.22656
V3	0.25625	-	-	0.25859	-	0.26094	0.26172	0.26563	-	0.25938
V4	0.2875	0.29063	0.28984	0.28906	0.28672	-	0.29219	0.29844	2.8828	0.28594
V5	0.3	0.3	0.30078	0.29922	0.29922	0.29922	0.3	0.30391	0.30078	-
V6	0.30859	0.31406	0.31172	0.31563	0.31484	0.32109	0.32422	0.32422	0.32266	0.31875
V7	-	-	-	-	-	-	-	-	-	-
V8	0.35703	0.36016	0.35938	0.35938	0.35547	0.35703	0.36172	0.36094	0.36094	0.35859
V9	0.37188	0.37266	0.37188	0.37266	0.37109	0.37344	0.37266	0.37266	0.37109	0.37344
V10	-	0.38516	0.38516	0.38516	0.38516	0.38438	0.38438	0.38359	0.38438	0.38438
V11	0.40078	0.4	0.40078	0.40156	0.40078	0.40234	0.39688	0.40078	0.39609	0.4
V12	0.47344	0.46953	0.46797	0.46953	0.47109	0.46953	0.47109	0.46875	0.47031	0.46875
V13	0.48047	0.48047	0.48359	0.48672	0.48203	0.48281	0.48047	0.48281	0.48359	0.48203
V14	0.5375	0.53672	0.53672	0.5375	0.53594	0.53672	0.5375	0.53672	0.53594	0.53516
V15	0.54375	0.54297	0.54297	-	0.54375	0.54375	-	0.54609	-	0.54297
V16	0.56406	0.56484	0.56641	0.56328	0.56484	0.56484	0.56406	0.56484	0.56563	0.56563
V17	0.56953	0.57031	0.56953	0.56953	0.56875	0.56797	0.56953	0.575	0.57109	0.57188
Mode	Sample11	Sample12	Sample13	Sample14	Sample15	Sample16	Sample17	Sample18	Sample19	
V1	0.1688	0.1633	0.1703	0.1695	0.1695	0.1648	0.1672	0.1641	0.1625	
V2	0.2289	0.2273	0.2266	0.2273	0.2289	0.2273	0.2273	-	-	
V3	-	0.2641	0.2648	0.2641	0.2617	-	0.2633	0.2570	-	
V4	-	-	0.2922	0.2914	0.2914	-	0.2844	0.2891	0.2914	
V5	0.3000	0.2992	0.3008	0.3008	0.3016	0.2992	0.2992	0.3008	0.2992	
V6	-	0.3211	0.3234	0.3234	0.3234	-	0.3195	0.3094	0.3148	
V7	-	-	-	-	-	-	-	-	-	
V8	0.3602	0.3625	0.3617	0.3633	0.3602	0.3578	0.3570	0.3594	0.3609	
V9	0.3742	0.3727	0.3742	0.3750	0.3727	0.3703	0.3750	0.3734	0.3719	
V10	-	0.3836	0.3844	0.3922	0.3844	-	0.3844	0.3859	-	
V11	0.3953	0.3953	0.4000	0.4000	0.3922	0.3938	0.3945	0.3953	0.3953	
V12	0.4695	-	0.4695	0.4695	-	0.4672	0.4750	0.4688	-	
V13	0.4820	0.4805	0.4805	0.4828	-	0.4813	0.4797	-	0.4797	
V14	0.5297	0.5281	0.5289	0.5289	0.5289	0.5250	0.5266	0.5289	0.5281	
V15	0.5375	0.5367	0.5375	0.5375	0.5375	0.5383	0.5367	0.5367	0.5367	
V16	0.5641	0.5656	0.5648	0.5664	0.5641	0.5617	0.5641	0.5648	0.5641	
V17	0.5695	0.5727	0.5781	0.5719	0.5742	0.5750	0.5734	0.5727	0.5703	

Table 8 Extracted natural frequencies (Hz) by FDD in lateral direction

Mode	Sample1	Sample2	Sample3	Sample4	Sample5	Sample6	Sample7	Sample8	Sample9	Sample10
L1	0.22734	0.22734	0.22813	0.22734	0.22578	0.22578	0.22656	0.22734	0.22656	0.22656
L2	0.25859	0.26094	0.26094	0.25938	0.25781	0.26094	0.26406	0.26563	0.26016	0.26016
L3	0.2875	0.29063	0.28984	0.28906	0.28516	0.28203	0.28906	0.28984	0.28828	0.28594
L3*	-	-	-	-	-	-	-	0.29844	-	-
L3**	-	-	-	-	-	-	-	-	0.31406	-
L4	0.30859	0.31406	0.31172	0.31563	0.31406	0.32109	0.32422	0.32422	0.32266	0.31563
L4*	-	-	-	-	-	-	-	-	-	-
L5	0.35469	0.36016	0.35625	0.36172	0.35391	0.35547	0.35938	0.37188	0.36016	0.35234
L5*	-	-	-	-	-	-	-	-	-	0.45234
L5**	-	-	-	-	-	-	-	-	-	0.51797
L6	0.5375	0.53672	0.53672	0.5375	-	-	0.5375	0.53594	0.53594	-
L7	0.56406	0.56563	0.56563	0.56328	0.56484	0.56484	0.56406	0.56484	0.56563	0.56484
Mode	Sample11	Sample12	Sample13	Sample14	Sample15	Sample16	Sample17	Sample18	Sample19	
L1	-	0.2164	0.2266	0.2273	0.2289	-	0.2227	0.2266	0.2273	
L2	0.2305	0.2641	0.2648	0.2641	0.2641	0.2328	0.2633	0.2570	0.2594	
L3	0.2813	0.2883	0.2922	0.2914	0.2914	0.2820	-	0.2891	0.2914	
L3*	-	-	-	-	-	-	0.3023	-	-	
L3**	-	-	-	-	-	-	-	-	-	
L4	0.3297	0.3211	0.3234	0.3219	0.3234	0.3203	0.3195	0.3141	0.3156	
L4*	0.3285	-	-	-	-	0.3383	-	-	-	
L5	0.3602	0.3547	0.3703	0.3633	0.3641	0.3578	0.3594	0.3594	0.3602	
L5*	-	-	-	-	-	-	-	-	-	
L5**	-	-	-	-	-	-	-	-	-	
L6	0.5531	0.5352	-	0.5375	0.5375	-	0.5367	0.5367	0.5367	
L7	0.5687	0.5656	0.5648	0.5664	0.5672	0.5563	0.5641	0.5648	0.5641	

## 5. Variation of dynamic characteristics induced by Typhoons

### 5.1 Typhoon-induced variation of natural frequency

In general, the natural frequencies of structures are varied according to ambient conditions (e.g.,

temperature and wind). Unfortunately, the measurement records provided from the research team at Hong Kong Polytechnic University do not include temperature data measured on site. Therefore, an alternative climate information recorded at a point near Hong Kong international airport was obtained from a website of Weather Underground (<http://www.wunderground.com>) as listed in Table 9. It is observed from the table that Samples 1-3, 7-10, and 12-13 were recorded under almost same temperature conditions while Samples 4-6 were recorded under a little higher temperature. It is further assumed that the temperature conditions did not make great influences to dynamic characteristics.

As shown in Fig. 22, typhoon-induced variations of natural frequencies were analyzed using the wind speed which were monitored by the WASHMS. The relationships between the natural frequencies and hourly mean wind speeds were examined for eight modes including four vertical modes (Modes V1, V5, V8 and V9) and four coupled torsional modes (Modes V2L1, V3L2, V4L3, and V7L5), as listed in Table 6. In the figure, the *Ref* indicates a natural frequency identified from Sample 2, which is the acceleration data measured under 'normal wind and light traffic condition'.

From Fig. 22, it is observed that the most sensitive mode with respect to the wind speed was Mode V7L5, and the maximum relative change of the natural frequency was 5.18%. Also, the least sensitive mode in term of the wind speed was Mode V9, and the maximum relative change of the natural frequency was observed as 0.21%.

Table 9 Climate information at measured time for each samples

Sample	Time	Temp. (°C)	Humidity (%)	State	*Wind Speed (m/s)
1	15:00-16:00, 28 Dec 1999	22	35	Sunny	2
2	15:00-16:00, 18 Feb 1999	25	57	Sunny	3.4
3	15:00-16:00, 01 Mar 1999	23	53	Sunny	3.34
4	15:00-16:00, 21 Jun 1999	30	74	Cloudy	3.41
5	15:00-16:00, 24 Jul 1999	34	56	Sunny	6.17
6	15:00-16:00, 12 Aug 1999	29	84	Weak rainy	4.2
7	03:00-04:00, 07 Jun 1999	26	94	Strong rainy	12.11
8	02:00-03:00, 23 Aug 1999	25	89	Rainy	15.62
9	06:00-07:00, 16 Sep 1999	25	94	Strong rainy	21.72
10	15:00-16:00, 16 Aug 1999	25	89	Weak rainy	15.91
11	08:00-09:00, 07 Jun 1999	27	94	Strong rainy	7.36
12	22:00-23:00, 16 Sep 1999	25	94	Strong rainy	7.77
13	09:00-10:00, 26 Sep 1999	24.5	94	Strong rainy	7.43

\* Wind speed is measured by WASHMS (Ni *et al.* 2015)

The natural frequencies of Modes V1 and V3L2 for other samples were higher than those for the *Ref.* The maximum relative changes of natural frequencies were 2.73% for Mode V1 and 1.76% for Mode V3L2. In the other way, the natural frequencies of Modes V2L1, V4L3 and V8 for other samples were lower than those for the *Ref.* The maximum relative changes of natural frequencies are 0.92% for Mode V2L1, 1.40% for Mode V4L3 and 1.27% for Mode V8. Except Mode V7L5, all modes have apparent trends of linear relationships (but with relatively low correlations) for the variations of natural frequencies.

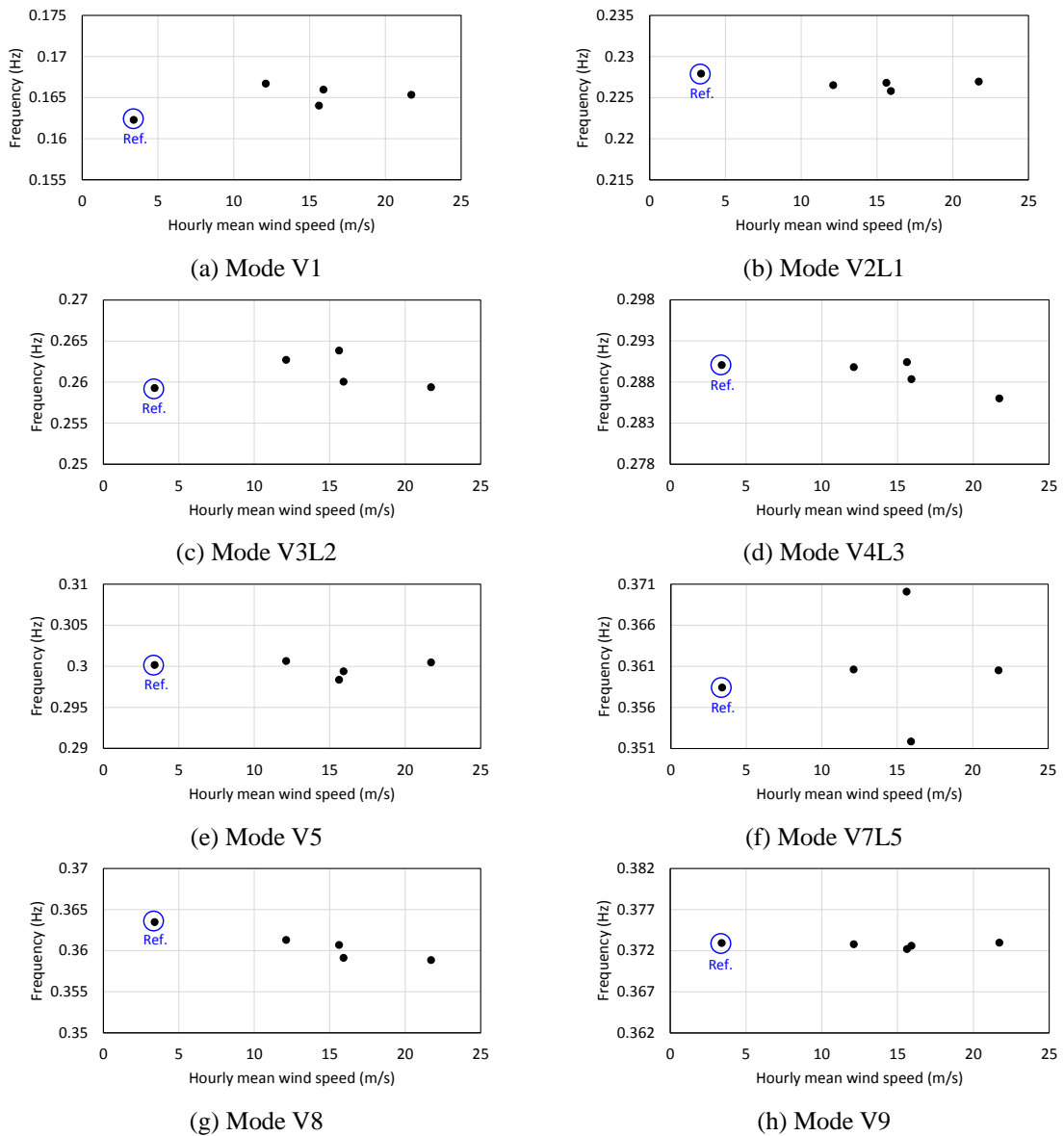


Fig. 22 Typhoon-induced variations of natural frequencies

Additionally, weak wind-induced variations of natural frequencies were investigated for four modes with the highest correlations (i.e., Modes V1, V2L1, V4L3 and V8) as shown in Fig. 23. In the figure, the variations of natural frequencies have no apparent trend with respect to the wind speed. Furthermore, temperature-induced variations of natural frequencies under the weak wind conditions were investigated as shown in Fig. 24. Note that *Ref.* was plotted for only the comparison with the others. As shown in the figure, correlations between the temperatures and the natural frequencies are low. From these observations, the frequency variations of the TKB should be analyzed considering the combined effects by the wind speed, temperature, and traffics.

### 5.2 Typhoon-induced variation of damping ratio

Figure 25 shows typhoon-induced variations of damping ratios of the TKB. In the figure, the *Ref* indicates a damping ratio identified from Sample 2. In the figure, the most sensitive mode for the wind speed is Mode V3L2, and the maximum relative change of the damping ratio is 202.05%. The least sensitive mode to the wind speed is Mode V8, and the maximum relative change of the damping ratio is 53.13%.

Compared to the *Ref*, the damping ratios of Modes V1, V4L3, V5, V7L5 and V9 have higher values for the other samples. The maximum relative changes of the damping ratios are 142.54% for Mode V1, 152.73% for Mode V4L3, 166.47% for Mode V5, 160.60% for Mode V7L5 and 71.70 % for Mode V9. In the other way, the damping ratios of Mode V2L1 for other samples have less values than ones for the *Ref*. The maximum relative change of the damping ratio is 72.99%. For the other modes, the variations of damping ratios have no apparent trend with respect to the wind speed.

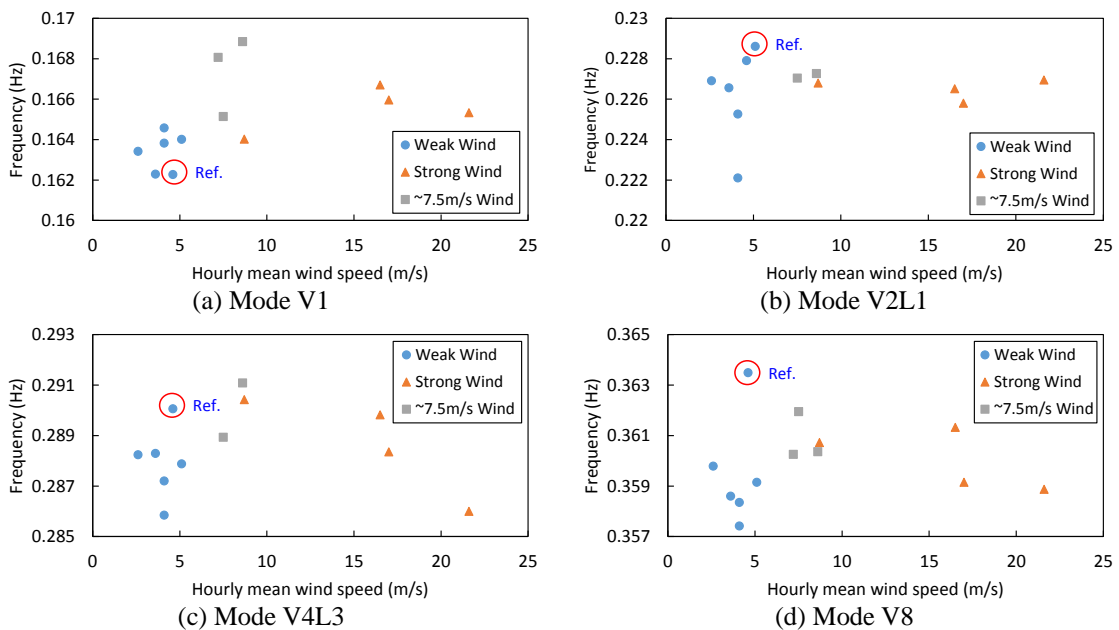


Fig. 23 Weak wind-induced variation of natural frequency

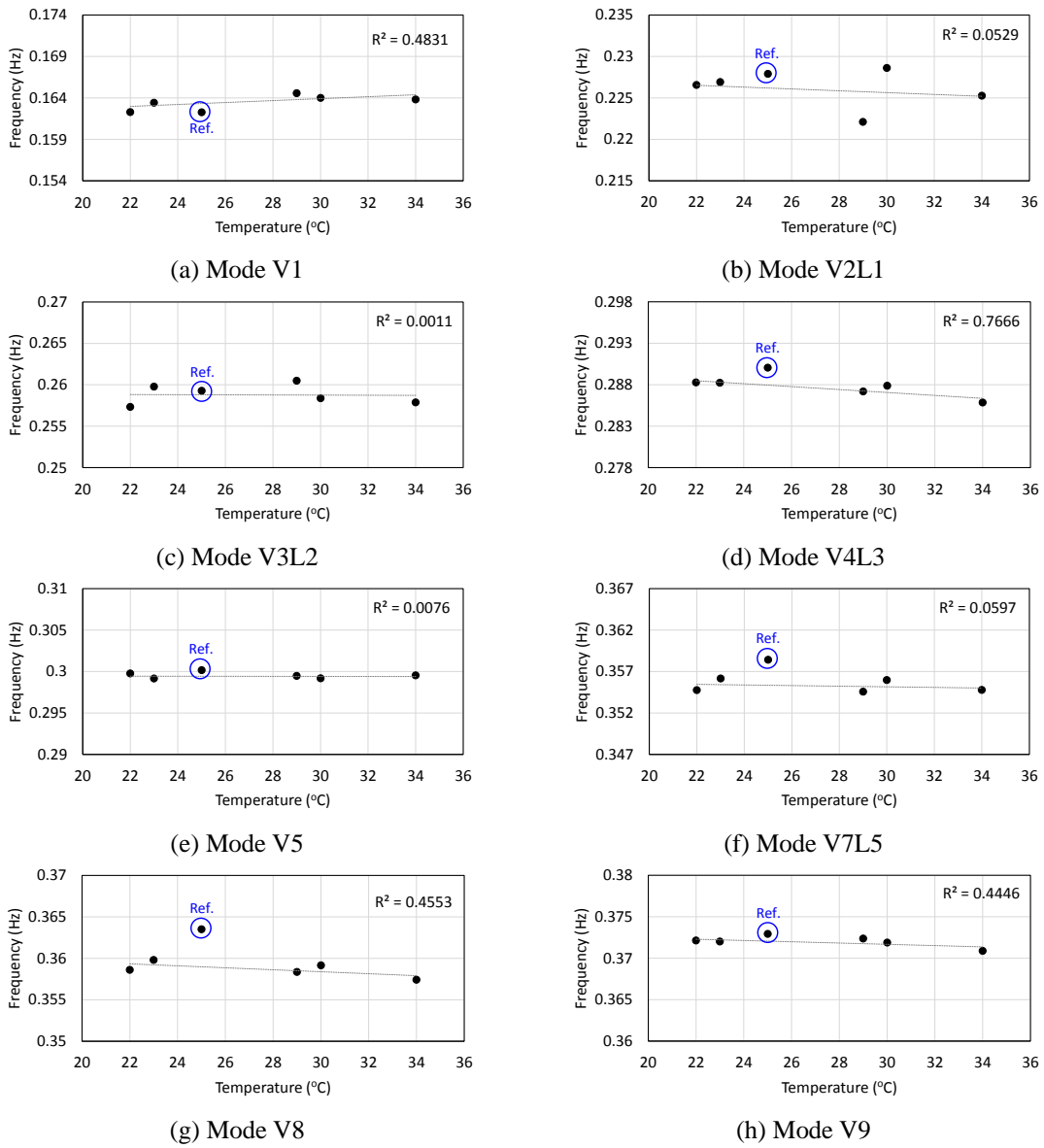


Fig. 24 Temperature induced-variation of natural frequency under weak wind condition

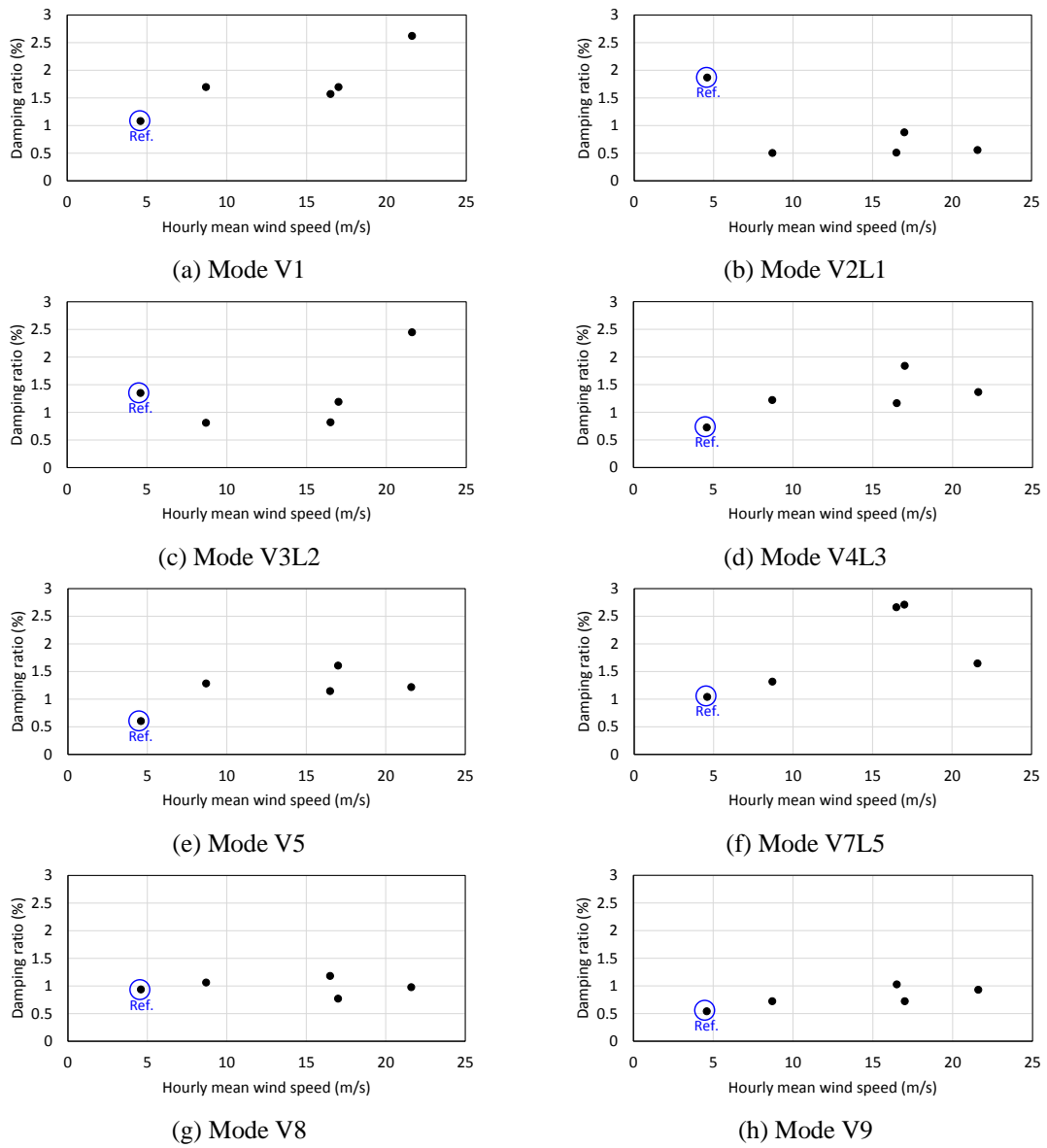


Fig. 25 Typhoon-induced variations of damping ratio

## 5. Conclusions

In this paper, the Ting Kau Bridge (TKB) under a series of excitation conditions (e.g., 19 samples of wind and traffic conditions) were examined to estimate the typhoon-induced variation of dynamic characteristics of the bridge. From the time-domain and frequency-domain analyses of the vibration records for the TKB, the nineteen samples could be categorized into three excitation conditions as 1) *normal wind and light traffic* condition, 2) *normal wind and heavy traffic* condition, and 3) *strong/typhoon wind* condition. Also, it was observed that acceleration levels under traffic conditions were larger than ones under typhoons, and the strong wind had dominant excitation frequencies less than 1 Hz while the traffic had dominant excitation frequencies above 1 Hz.

By using the frequency-domain decomposition (FDD) method and the stochastic subspace identification (SSI) method, seventeen modes in the vertical direction and seven modes in the lateral direction were identified. With compared to a published report, one additional coupled torsional mode was found by extracting modal parameters separately in the vertical and lateral directions. The vertical mode shapes extracted by the FDD method for relatively higher modes have very low accuracy in the *strong/typhoon wind* conditions and also ones for lower modes have relatively low accuracy in the *normal wind* conditions. From those observations, the time-domain SSI method was more reliable than the frequency-domain FDD method when modal parameters of the TKB were extracted by using ambient test records under various wind conditions.

Typhoon-induced variations of natural frequencies and damping ratios were examined on eight modes which included four vertical modes and four coupled torsional modes. The coupled torsional modes were relatively sensitive to the wind speed as compared to the vertical modes. With the increase of wind speed, natural frequencies exhibited decreasing (or no particular) trends in the coupled torsional modes, but increasing, decreasing (or no particular) trends in the vertical modes. The maximum relative change of natural frequency was about five percent during typhoon conditions. Modal damping ratios exhibited complex trends without any particular patterns with respect to wind speeds and natural frequencies.

## Acknowledgements

This work was supported by Basic Science Research Program through the National Research Foundation of Korea (NRF) funded by the Ministry of Education, Science and Technology (NFR-2013R1A1A2A10012040). The graduate student and BK21Plus professor involved in this research were also partially supported by the Brain Korea 21 Plus program of Korean Government. The authors greatly appreciate Prof. Y.Q. Ni at Hong Kong Polytechnic University for inviting us in this research for the benchmark test.

## References

- Askegaard, V. and Mossing, P. (1988), "Long term observation of RC-bridge using changes in natural frequencies", *Nordic Concrete Res.*, **7**, 20-27.
- Bendat, J.S. and Piersol, A.G. (1993), *Engineering applications of correlation and spectral analysis*, New York, NY, Wiley-Interscience.

- Brincker, R., Zhang, L. and Andersen, P. (2001), "Modal identification of output-only systems using frequency domain decomposition", *Smart Mater. Struct.*, **10**, 441-445.
- Brownjohn, J.M.W., Magalhaes, F., Caetano, E. and Cunha, A. (2010), "Ambient vibration re-testing and operational modal analysis of the Humber Bridge", *Eng. Struct.*, **32**, 82003-2018.
- Chen, J., Xu, Y.L. and Zhang, R.C. (2004), "Modal parameter identification of Tsing Ma suspension bridge under typhoon Victor: EMD-HT method", *J. Wind Eng. Ind. Aerod.*, **92**, 805-827.
- Hermans, L. and Van Der Auweraer, H. (1999), "Modal testing and analysis of structures under operational conditions: industrial applications", *Mech. Syst. Signal Pr.*, **13**(2), 193-216.
- Ho, D.D., Nguyen, K.D., Yoon, H.S. and Kim, J.T. (2012a), "Multiscale acceleration-dynamic strain-impedance sensor system for structural health monitoring", *Int. J. Distributed Sensor Networks*, **2012**, 1-17.
- Ho, D.D., Lee, P.Y., Nguyen, K.D., Hong, D.S., Lee, S.Y., Kim, J.T., Shin, S.W., Yun, C.B. and Shinozuka, M. (2012b), "Solar-powered multi-scale sensor node on Imote2 platform for hybrid SHM in cable-stayed bridge", *Smart Struct. Syst.*, **9**(2), 145-164.
- Hong, D.S., Nguyen, K.D. Lee, I.C. and Kim, J.T. (2012), "Temperature-compensated damage monitoring by using wireless acceleration-impedance sensor nodes in steel girder connection", *Int. J. Distributed Sensor Networks*, **2012**(167120), 1-12.
- Huynh, T.C., Park, Y.H., Park, J.H., Hong, D.S. and Kim, J.T. (2015), "Effect of temperature variation on vibration monitoring of prestressed concrete structures", *J. Shock Vib.*, **2015**, 1-9.
- Ibrahim, S.R. and Mikulcik, E.C. (1977), "A method for the direct identification of vibration parameters from the free response", *Shock and Vibration Bulletin*, 47(4), pp. 183-198.
- Juang, J.N. and Pappa, R.S. (1985) "An eigensystem realization algorithm for modal parameter identification and model reduction", *J. Guidance*, **8**(5), 620-627.
- Karbhari, V.M. and Ansari, F. (2009), *Structural health monitoring of civil infrastructure systems*, Woodhead Publishing Limited, Cambridge, UK.
- Kim, J.T., Huynh, T.C. and Lee, S.Y. (2014), "Wireless structural health monitoring of stay cables under two consecutive typhoons", *Struct. Monit. Maint.*, **1**(1), 47-67.
- Kim, J.T., Park, J.H., Hong, D.S. and Ho, D.D. (2011), "Hybrid acceleration-impedance sensor nodes on Imote2-platform for damage monitoring in steel girder connections", *Smart Struct. Syst.*, **7**(5), 393-416.
- Kim, J.T., Park, J.H. and Lee, B.J. (2007a), "Vibration-based damage monitoring in model plate-girder bridges under uncertain temperature conditions", *Eng. Struct.*, **27**(7), 1354-1365.
- Kim, J.T., Park, J.H., Yoon, H.S. and Yi, J.H. (2007b), "Vibration-based damage detection in beams using genetic algorithm", *Smart Struct. Syst.*, **3**(3), 263-280.
- Kim, J.T., Yun, C.B. and Yi, J.H. (2003), "Temperature effects on frequency-based damage detection in plate-girder bridges", *J. Civil Eng. - KSCE*, **7**(6), 725-733.
- Koo, K.Y., Lee, J.J., Yun, C.B. and Kim, J.T. (2009), "Damage detection in beam-like structures using deflections obtained by modal flexibility matrices", *Adv. Sci. Technol.*, **56**, 483-488.
- Magalhaes, F., Caetano, E. and Cunha, A. (2007), "Challenges in the application of stochastic modal identification methods to a cable-stayed bridge", *J. Bridge Eng. - ASCE*, **12**(6), 746-754.
- Min, Z., Sun, L. and Dan, D. (2009), "Analysis of wind-induced response and dynamic properties of cable-stayed bridge under typhoon", *Jo. Tongji University (Natural Science)*, **2009**(9), 1139-1145.
- Ni, Y.Q., Ko, J.M., Hua, X.G. and Zhou, H.F. (2007), "Variability of measured modal frequencies of a cable-stayed bridge under different wind conditions", *Smart Struct. Syst.*, **3**(3), 341-356.
- Ni, Y.Q., Wang, Y.W. and Xia, Y.X. (2015), "Investigation of mode identifiability of a cable-stayed bridge: comparison from ambient vibration responses and from typhoon-induced dynamic responses", *Smart Struct. Syst.*, **15**(2), 447-468.
- Overschee, V.P. and De Moor, B. (1996), *Subspace Identification for Linear Systems*, Kluwer Academic Publisher.
- Park, J.H., Huynh, T.C. and Kim, J.T. (2015), "Wireless monitoring of typhoon-induced variation of dynamic characteristics of a cable-stayed bridge", *Wind Struct.*, **20**(2), 293-314.

- Rohrmann, R.G., Baessler, M., Said, S., Schmid, W. and Ruecker, W.F. (2000), "Structural causes of temperature affected modal data of civil structures obtained by long time monitoring", *Proceedings of the 18th International Modal Analytical Conference*, San Antonio, Texas, USA.
- Siringoringo, D.M, and Fujino, Y. (2008), "System identification of suspension bridge from ambient vibration response", *Eng. Struct.*, **30**(2), 462-477.
- Sohn, H., Farrar, C.R., Hemez, F.M., Shunk, D.D., Stinemates, D.W. and Nadler, B.R. (2003), *A Review of Structural Health Monitoring Literature: 1996-2001*, Los Alamos National Laboratory Report, LA-13976-MS, Los Alamos, NM.
- Yi, J.H. and Yun, C.B. (2004), "Comparative study on modal identification methods using output-only information", *Struct. Eng. Mech.*, **17**(3-4), 445-446.